Diploma Thesis

Methods to measure optical properties of mirror facets for CTA

performed at the
Erlangen Center for Astroparticle Physics
University of Erlangen-Nürnberg

by
André Wörnlein

supervisor:
Prof. Dr. Christian Stegmann

second reader:
Prof. Dr. Christopher van Eldik

Erlangen, July 9, 2012

Abstract

In this thesis, different methods to measure the optical properties of mirror facets for the Cherenkov Telescope Array were investigated. For measuring the Point Spread Function (PSF) of these mirrors, two methods, the so called 2f-measurement and the Phase Measuring Deflectometry (PMD), were compared. It could be shown, that the results for both methods are in a good agreement. Reasons for the most prominent differences of both methods could be found and eliminated. Because it could be shown, that PMD leads to equivalent results as the well understood 2f-method, a new field of application for this method could be opened up. The possibility of PMD to measure in a very compact setup, gave the opportunity to measure the behavior of mirror prototypes in a climate chamber under different temperatures. The unpredictable difficulties with using PMD under extreme conditions could be defined and solutions could be developed. The already existing 2f-setup was enhanced that it was possible to measure the reflectivity of mirror facets as well. Though there are in all fields still difficulties to overcome, this thesis was a step forward to establish a testing facility for the optical properties of mirrors for Cherenkov Telescopes in Erlangen.

Zusammenfassung

In dieser Arbeit wurden verschiedene Methoden untersucht um die optischen Eigenschaften von Spiegelfacetten für das Cherenkov Teleskop Array (CTA) zu testen. Um die Point Spread Function (PSF) dieser Spiegel zu untersuchen, stehen zwei Mehtoden, die so genannte 2f-Methode und die Phasenmessende Deflektometrie (PMD), zur Verfügung. Es konnte gezeigt werden, dass die Resultate beider Methoden in guter Übereinstimmung zu einander stehen. Die Ursachen der größten Unterschiede zwischen beiden Methoden konnten gefunden und eliminiert werden. Da gezeigt werden konnte, dass PMD gleichwertige Ergebnisse zur gut verstandenen 2f-Methode liefert, konnte ein neues Anwendungsgebiet erschlossen werden. Die Fähigkeit von PMD in einem sehr kompakten Aufbau Messungen duchzuführen, ergab die Möglichkeit das Verhalten von Spiegelprototypen in einer Klimakammer unter verschiedenen Temperaturbedingen zu messen. Die unvorhersehbaren Schwierigkeiten, PMD unter extremen Bedingungen zu verwenden, konnten bestimmt und Lösungen gefunden werden. Der bereits existierende 2f-Aufbau konnte erweitert werden, so dass es ebenfalls möglich ist, die Reflektivität von Spiegelfacetten zu vermessen. Obwohl in allen Bereichen immernoch Schwierigkeiten zu überwinden sind, ist diese Arbeit ein Schritt in dem Bestreben, in Erlangen eine Testeinrichtung für optische Eigenschaft von Spiegeln für Cherenkov Teleskope zu etablieren.

Contents

Chapter 1

The Cherenkov Telescope Array

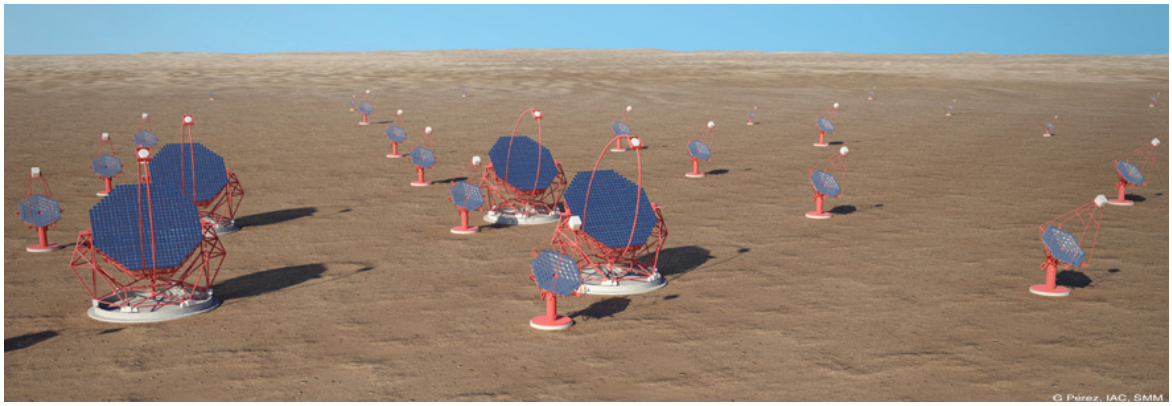

Figure 1.1: Artistic view of CTA [1],[G.Pérez, IAC,SMM]

The Cherenkov Telescope Array (CTA) is an international collaboration with more than 1,000 members out of 27 countries. The goal of this collaboration is to construct an array of Imaging Air Cherenkov Telescopes (IACT) to observe the universe at very high energy. To reach this goal, it is planned to build an array on the southern hemisphere consisting of up to 100 single telescopes. To be able to observe the whole sky it is also planned to build a smaller array of telescopes on the northern hemisphere.
There will be three different sizes of telescopes to observe different energy ranges. To observe the low energy range (10GeV-100 GeV) there will be a few (3-6) Large Sized Telescopes (LST) in the center of the array, which will have a diameter of about 24 m. To observe the medium energy range (100GeV-1TeV) there will be a number of medium sized telescopes (MST). For the very high energy range (more than 10 TeV) there will be lots of small sized telescopes (SST).
Since the whole project is still in the preparatory phase the final design of the array and the telescopes is not yet settled.[1]

1.1 Imaging Air Cherenkov Telescopes

The CTA collaboration constructs an observatory to detect the γ-radiation of the universe in the very high energy range. To do so there are two possibilities. Due to the fact that the atmosphere of the Earth is opaque for these γ-rays, it is not possible to observe them directly with a ground-based telescope. To overcome this problem one could launch a satellite and observe the sky from above the atmosphere. This solution has the drawback that the size of a satellite is limited and so the observation area is quite small.
The second possibility is to observe γ-rays indirectly via so called Cherenkov light. If high energetic photons hit the atmosphere, these photons create a so called airshower consisting of several different particles in the upper atmosphere. These secondary particles emit Cherenkov light, which occurs if the speed of the particle is larger than the speed of light in the medium in which the particle is moving. The Cherenkov light is emitted in a wavelength range between 300 nm and 600 nm with a maximum at 400 nm and can be detected by a IACT.

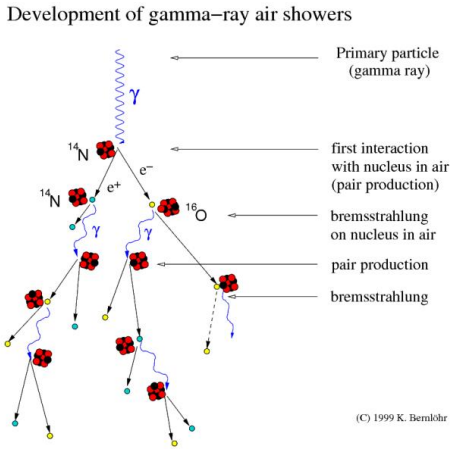

Figure 1.2: Scheme of a atmospheric shower induced by a cosmic photon

The emitted Cherenkov light is forming a cone in the atmosphere and illuminates the ground (see fig. 1.3 a) This Cherenkov light then is focused by a mirror dish into a camera consisting of photo-multipliers.
If the emitted Cherenkov light is detected by one single telescope (see fig. 1.3 b) the light will create a picture on the camera like in fig. 1.4 a. Out of the shape and the orientation of the image the direction and the energy of the original photon can be determined. To get a better result it is helpful to combine pictures of more telescopes. This is possible by constructing more telescope so close together that they can be illuminated by the same Cherenkov cone (see fig. 1.3 c). By superimposing these pictures one can get a more precise result. The resulting picture would look like in fig. 1.4 b.

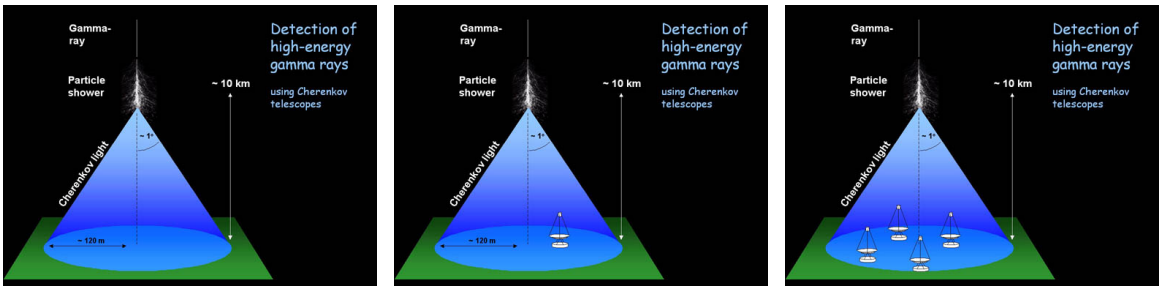

(a) Cone of cherenkov light in the atmosphere hitting the ground (b) Cherenkov light detected by one telescope (c) Cherenkov light detected by four telescopes

Figure 1.3: Cherenkov cone in the atmosphere and its detection.

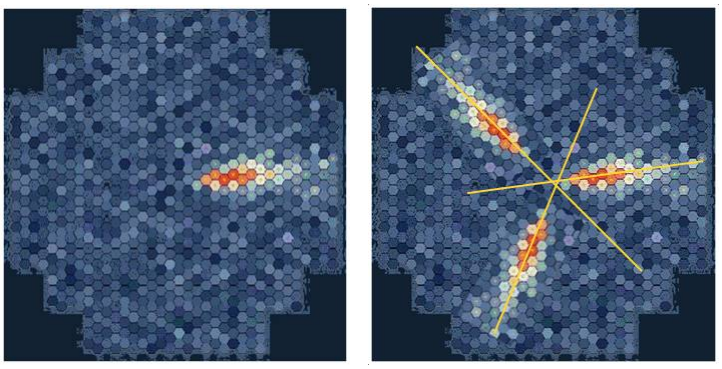

(a) detection by one telescope (b) detection by two telescopes

Figure 1.4: Pictures of detected Cherenkov light on the camera

Due to the fact that the emitted Cherenkov light is faint the reflecting area has to be huge. As it is expensive and technologically complicated to produce single tile mirrors of the needed size, the decision was made to produce many small mirror tiles and combine them on the telescope to get a full dish. This technology is used for all already existing IACTs like the High Energy Stereoscopic System (HESS) and the Major Atmospheric Gamma-ray Imaging Cherenkov telescopes (MAGIC).
The construction of such a telescope is expensive. The telescope has to be able to carry the weight of the mirrors in a stable and repeatable way. To reduce the costs of such a construction it is needed to reduce the weight of the mirrors. This led to the decision to develop composite mirrors and not use massive glass mirrors.
For the three different telescope types there will be three different types of mirrors. For the LST there will be hexagonal mirrors with a size of 1.50 m flat to flat. For the MST mirrors will also be hexagonal with 1.20 m flat to flat. For SST there is no final design decision yet. The mirrors will be fixed on the telescopes via three pads on the backside. One of these pads will be fixed with the telescope directly and the other two pads will be fixed via a motor in between. So it will be possible to move the mirrors directly on the telescope with just moving the actuators, the positioning unit between the mirror and the telescope.

1.2 Mirrors for CTA

Not only to reduce the weight of the mirrors, but also the costs, the idea of using massive glass mirrors had to be abandoned. The general idea is to construct the mirrors in the way that the glass layer is as thin as possible and supported by an underlying honeycomb structure.
The whole CTA project is still in the research and development phase. So there was not yet made a decision which technology will be used to produce the mirrors.

1.2.1 Mirror technology

The most promising mirror producing technologies are all based on the same principle. A sketch of this principle can be seen in fig. 1.5.

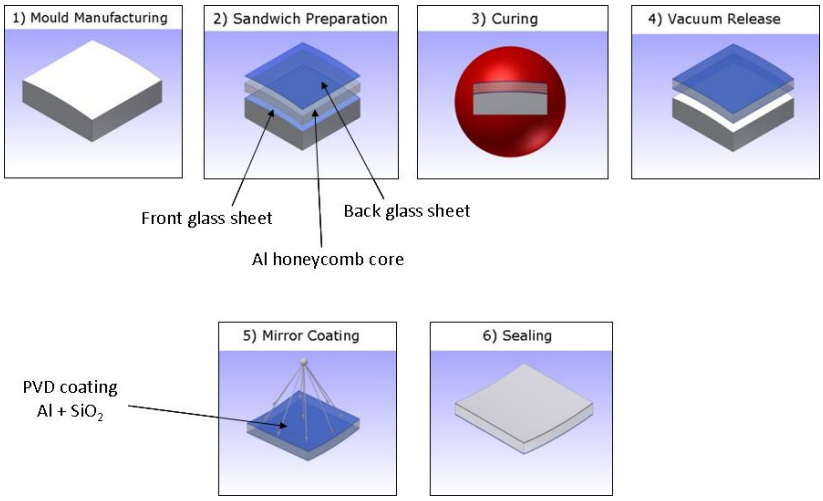

Figure 1.5: Sketch of the mirror producing principle using the example of INAF Brera represented by Giovani Pareschi. [2]

The mirrors are produced in different steps. First of all a mold is constructed, which is spherical and has exactly the radius of curvature that the resulting mirror will have (see fig. 1.6 a).
On this mold a glass sheet, a honeycomb structure and an additional glass sheet are pressed and in this way curved in the right way.
This procedure is called slumping (see fig. 1.6 b). One can distinguish between two different ways of slumping, the so called cold slumping and hot slumping. Cold slumping means that the glass sheet is already cooled down after the producing and then pressed on the mold. Hot slumping means that the glass sheet is still hot during the pressing process. The underlying honeycomb structure can as well be curved with the help of the mold or being constructed directly in a curved way. The slumping process is happening under vacuum conditions so no air bubbles can stay between the mold and the glass sheet. The components are glued together and a sandwich structure forms (see fig. 1.6 c).

Now the glue has to dry and the sandwich structure has to stabilize itself. This is called curing and it strongly depends on the used materials how the sandwich is cured.

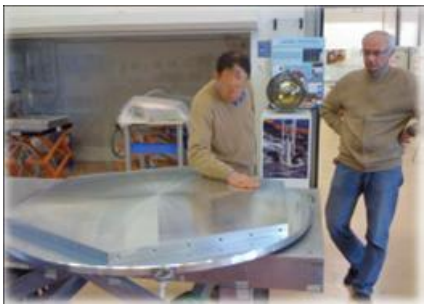

(a) Mold that is used at CEA Saclay represented by Pierre Brun

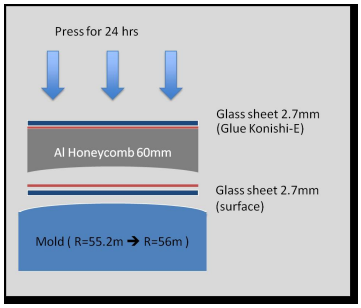

(b) Sketch of coldslumping procedure in Japan represeted by Masahiro Teshima

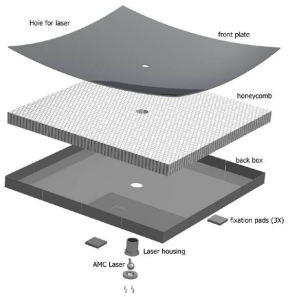

(c) Sandwich structure using the example of MAGIC mirrors produced at INAF Brera

Figure 1.6: Slumping technology.[2]

After releasing the vacuum the result is still a non-reflective sandwich.
The upper surface now has to be coated with a reflective substrate. This is done in a coating chamber under high vacuum (see fig. 1.7 a). A reflective layer and a protection layer of SiO_2 are distributed on the surface. By introducing more reflective and protective layers the durability and reflectivity of the mirror can be improved. The reflective material differs between the different technologies. The wavelength range in which the mirror is reflecting can be modified by changing the material of the reflective layer (see fig. 1.7 b).

(a) Coating chamber

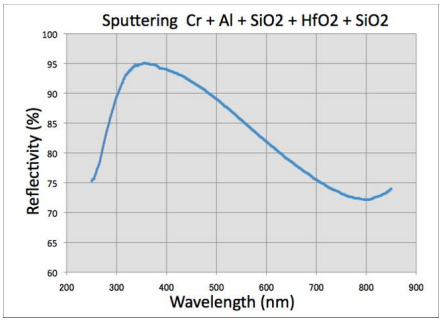

(b) Coating example with different substrates and resulting reflectance curve

Figure 1.7: Coating technology using the example of the Japanese mirror producing technology [2]

Now the mirror could be used, but its durability is not high. In difference to a "home-use" mirror, the reflective layer is on top of the mirror and not on the backside. To protect this layer, the mirror has to be sealed. This is done by introducing some more SiO_2 layers on

the surface.
Now the mirror is ready to use and its optical performance can be tested.

1.2.2 Mirror requirements

Two important features have to be checked for all mirrors. One is the focussing property of the mirrors. To check this, the so called Point Spread Function (PSF) is observed. The PSF means the size of the reflected spot of a point-like light source. If the mirror is illuminated with a point-like light source the light is reflected and focused by the mirror. The size of the reflected spot defines the PSF of the mirror. To get a comparable value of this size a so called d80 is defined. D80 means the diameter of a circle that contains 80% of the reflected light. The requirement for CTA mirrors is that this circle has to fit into the photomultiplier tubes on the camera of the telescope. So the d80 circle shall not exceed 1/3 of the pixel size of the cameras. Since the diameter of the photomultiplier tubes for MST and LST is 50 mm, the PSF has to be smaller than 17 mm to fulfill these requirements.
The second property of the mirrors that has to be checked is the focused reflectivity. Since the telescopes are constructed to observe Cherenkov light more than 85% of the light hitting the mirrors has to be reflected and focused in a wavelength range between 300 nm and 600 nm. Focused means in this case that 85% of the light hitting the mirror has to end up in a circle that has a diameter of maximum 2/3 of the pixel size of the camera.[3]
CTA will be an outside facility, so the telescopes and the mirrors will have to stand different environmental conditions. Therefore the optical properties have to be stable in a temperature range betwen $-10°$ C up to $+30°$ C. For these requirements, different testing methods were developed and will be described in the next chapter.

Chapter 2

Testing methods for Mirrors

2.1 Classical 2f-approach

The mirrors are constructed to observe light, that comes out of the atmosphere from about 10 km height, which can be assumed as infinity. That means, the rays of light can be assumed as parallel. So light coming from this distance will be focused at the focal distance (f) of the specific mirror. To test the required properties of the mirrors, this situation must be simulated. In general you need either a light source that is at least 10 km far away from the mirror, or a light source that distributes parallel light and is big enough to illuminate the whole mirror. Both cases are very difficult to realize.
To overcome these problems, another method was developed. The so called 2f-method takes advantage of the fact, that light, that is distributed from a point-like source, will be focused by the mirror. If the light source is positioned exactly at the distance of twice the focal length of the mirror (so in 2f-distance), the light will be focused in this point. That means that you can directly see and measure the PSF of the mirror near the light source. As a result you can construct a compact setup to measure the size and intensity of the focused spot.

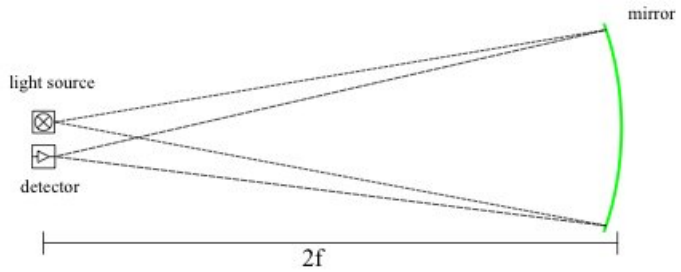

Figure 2.1: Sketch of the 2f measurement setup. The distance between the light source and the detector is shown extremely increased to demonstrate the light rays more clearly; picture from [7].

By introducing a slight tilt on the mirror, the reflected light can be mapped next to the light source. In that way the PSF can be observed directly. For this purpose we have constructed a mirror holder, on which the mirrors can be placed vertically and fixed. Due to the fact that the mirrors tested up to date are still prototypes, not every mirror has pads for fixing on the backside. So a solution had to be found to mount the mirrors without these pads but keep the movability. This could be realized with a holder on which the mirrors were laying on a base-bar of a frame. With the help of two motors on the backside, it is possible to introduce a tilt on the mirror. So you can position the PSF in a very easy way. The actual setup used in Erlangen consist of a red light emitting diode (LED) and a ground glass. For taking the pictures a charge-couple device (CCD) camera, a $NikonD3100$, is used. See the setup in fig. 2.2.

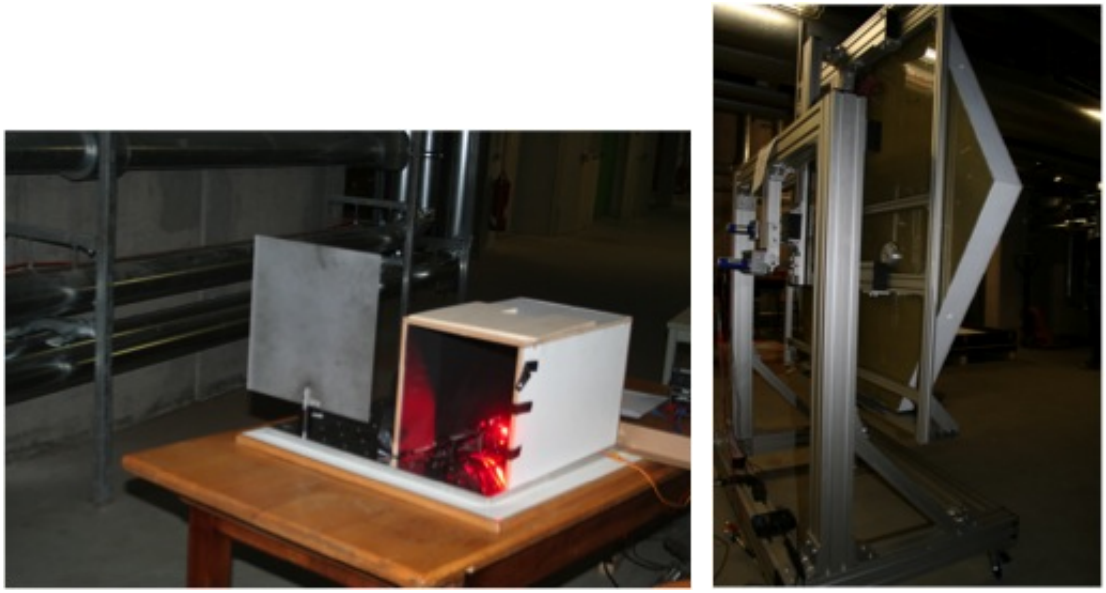

(a) Light source and screen, camera is not visible on this picture

(b) Mirror holder with mounted mirror and motors on the backside

Figure 2.2: Setup used in Erlangen to measure the PSF in 2f-distance.

The used LED emits red light with a wavelength of 650 nm. By introducing two lenses and a aperture in front of this LED, it was possible to make the light distribution very homogeneous. The fluctuation of intensity within the whole emitted spot is in the range of 2%. The light distribution properties of the used LED are shown in fig. 2.3.

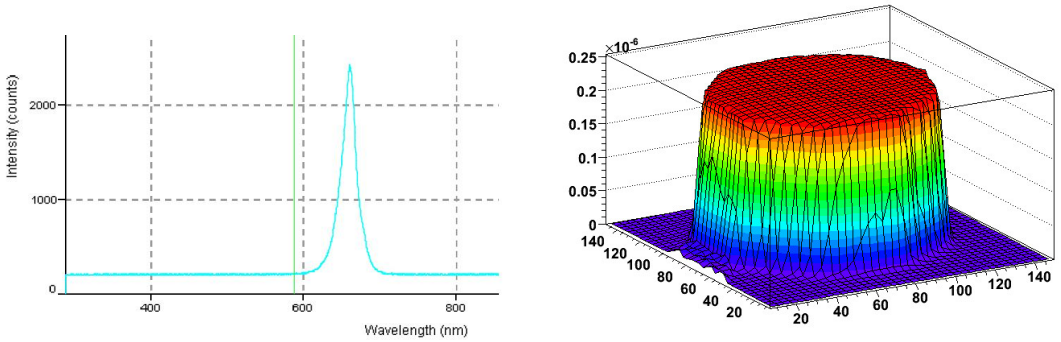

(a) Spectrum of the emitted light

(b) Homogeneity of the spot emitted by the LED taken in 2 meter distance. X- and y-axis show spot extension in mm, z-axis shows intensity in Ampere

Figure 2.3: Light distribution properties of the used LED

The commercially available NIKON D3100 has a 40 mm objective. This camera has a 23.1 mm by 15.4 mm big complementary metal-oxide-semiconductor (CMOS) chip with a resolution of 4608 pixels by 3072 pixels. This leads to a pixel size of 5 μm by 5 μm.[8].

2.2 Phase Measuring Deflectometry

Phase Measuring Deflectometry (PMD) is a technique to measure the properties of specular surfaces. It has been developed by the Optical Sensing, Metrology and Inspection (OSMIN) group of prof. Gerd Häusler at the University of Erlangen and is described in detail in [4], [5] and [6]. PMD is a well established tool to examine specular surfaces such as progressive eyeglasses, windshields and painted car bodies. For these purposes, PMD is already used very successfully in industry.
The basic idea of PMD is to observe the distortions of a defined pattern after it has been reflected by the illuminated surface (see fig. 2.4). From these distortions one can calculate the exact local slope in each camera pixel and the corresponding curvature and shape of the surface by numerical differentiation and integration, respectively.
To realize this, a sinusoidal pattern of black and white stripes is first projected on a screen, then reflected by a specular surface and last observed by a camera. Out of the distortions of this pattern, the local slope of the surface can be determined.

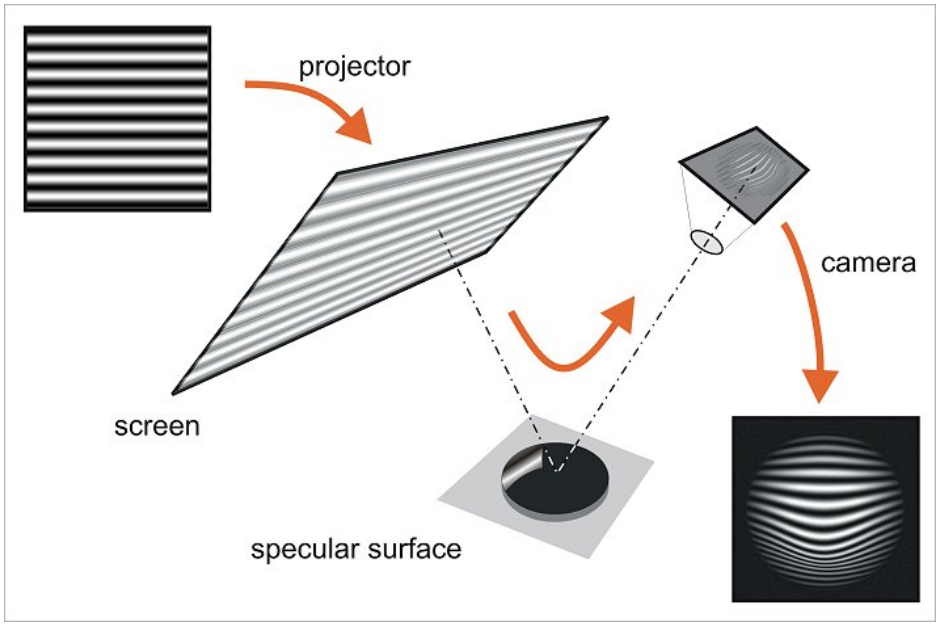

Figure 2.4: Sketch of the measurement principle of PMD. The sinusoidal pattern is projected on a screen or a ground glass. The camera takes pictures of the distortions of the pattern after the reflection on the object; picture from [4].

2.2.1 Principle of PMD measurements

This chapter mainly follows the description of PMD given in [4].
The general idea of PMD is to observe the reflection of a regular pattern on a specular surface. Reflection on such a surface is mainly defined by the normals of the surface. The angle of incidence Θ_i and the angle of reflection Θ_r are equal with the surface normal as baseline (see fig. 2.5). This means that one can determine the normal on every point of a surface, if the reflective behavior is known.

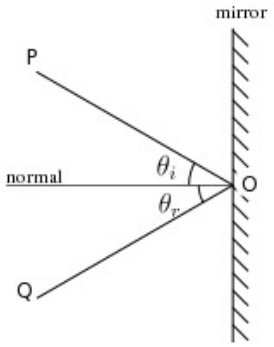

Figure 2.5: Principle of specular reflection. The angle of incidence and the angle of reflection are equal.

The normals of the object or the resulting slope can be seen as the primary measurand. Out of this, the surface shape and curvature can be determined via integration or differentiation. To learn something about the reflective behavior of the surface, the camera has to be able to observe the pattern on the whole surface. A solution for this problem is to choose a big screen, which is diffusely emitting. With such a device you can make sure that the whole observed surface is illuminated in a proper way.
To figure out how the projected pattern is distorted by the surface the part of the pattern that is observed by the camera has to be distinguished. This means, the pixel of the screen that can be seen on a specific part of the surface has to be identified. To make this possible, the position on the screen is encoded in the phase of the sinusoidal pattern. To make this encoding unique, it is needed to not just project a single pattern, but to perform a phase shift. By shifting the vertically projected phase of the pattern in x-direction, the x-value of the position is encoded. By shifting the horizontally projected pattern in y-direction, the y-value is encoded analog. How this observation is done can be seen in fig. 2.6.
Using a sinusoidal pattern has the big advantage, that the phase is conserved, even if the screen is observed out of focus. Since it is not possible to focus on both„ the screen and the specular surface, the camera is focused on the specular surface to get a better lateral resolution for the surface data. But focusing on the specular surface leads to the problem, that the contrast of the observed pattern is decreased. Therefore the lateral and the angular resolution are coupled and an uncertainty limit can be determined. A sketch of the focusing in a PMD setup can be seen in fig 2.7.

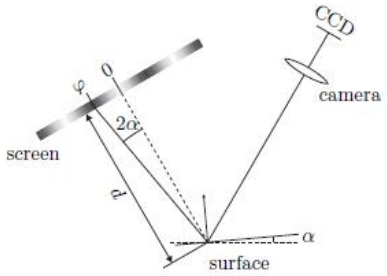

Figure 2.6: Observation of the screen via a specular surface. The phase ϕ is a measure for the local slope α. Picture from [6]

This relation between the uncertainty of the slope measurement $\delta\alpha$ and laterally resolvable distance δx is calculated in [6] and is

$$\tan \delta\alpha * \delta x = \frac{\pi\lambda}{Q} \tag{2.1}$$

with λ as mean wavelength of the screen and Q as a quality factor that comes from properties of the used camera and describes the phase uncertainty caused by the camera quantization error and photon noise [6].

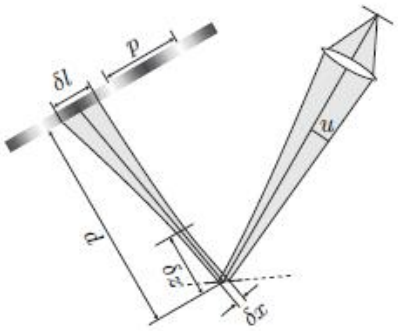

Figure 2.7: Principle of focusing on the specular surface. The depth of focus δz is shorter than the distance between object and screen and the contrast decreases. So the period p must be longer than the diameter of the circle of confusion δl. Picture from [6]

To determine the local slope of the surface, it is crucial to know the exact position of the screen and the camera, and the optical properties of the camera itself. Therefore one has to calibrate the setup.

2.2.2 Calibration of a PMD setup

All components of the setup have to be calibrated. This means the screen, the camera and the position of both to each other.

Calibration of the screen

For PMD measurements it is assumed that the screen is perfect and completely flat. In reality this is not the case, so the properties of the screen have to be checked. In general there are three different properties to check: The slope of the screen, the homogeneity of the light distribution and the pixel size respectively the resolution of the screen.
The slope of the screen is investigated by projecting a marked grid on the screen and observe this with a previously calibrated camera from different angles. An example for such a dotted pattern can be seen in fig. 2.8. Due to the fact, that a straight line will stay a straight line even if observed under different angles, it is possible to check the slope of the screen with photometric methods. For this purpose the commercially available program called *australis* was used. This program could determine the surface properties out of the distribution of the marks on the screen by comparing the pictures of the marks from different angles. This data can be directly implemented into the PMD-program called $softPMD$.

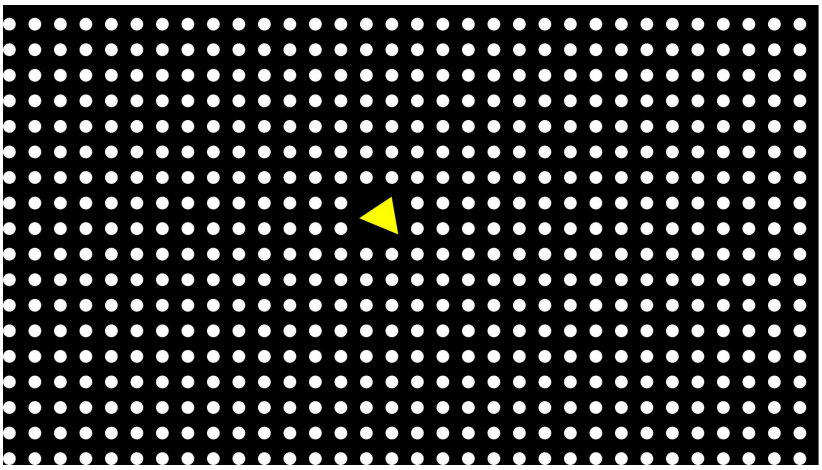

Figure 2.8: Example of a dotted screen image to project on the screen and calibrate its surface shape. The yellow triangle is needed to position the marks on a taken image.

The homogeneity of the screen can be checked with a CCD camera or with a scanning device equipped with a photodiode. Out of this data one can create a light distribution map and change the projected pattern in this way that the pattern will be homogeneous. This change can as well be implemented directly into $softPMD$.
The last point is the most tricky one, because one has to verify the actual size of the screen, the size of the single pixel and the number of pixels visible on the screen very precisely. Since now there is no established routine how to perform this calibration but a possible approach would be to measure the pixel size with a microscope.

Calibration of the cameras

The camera itself has to be calibrated as well. PMD assumes that the camera is a perfect pinhole-camera, but in reality this is not the case. The image observed by the camera is distorted by the objective, imperfections of the CCD-chip and other geometric disturbances. For this purpose, a similar approach was used as for calibrating the screen. A plate with similar marks as in fig. 2.8 was placed in front of the camera and several pictures were taken observing the plate from different angles. Now it is assumed that the target is perfect and all distortions of the grid are caused by the camera. For this case *australis* is able to calculate parameters to get rid of these distortions. These parameters can as well be implemented directly into $softPMD$.

Calibration of the positions

For good results the positions of the screen and the cameras are needed to be known very exactly. For this purpose, a calibration routine was developed that worked with a sphere inside the setup, which is assumed to be perfect. A spherical mirror is put inside the setup and the sinusoidal pattern is observed via this sphere. Afterwards this mirror moved inside the setup and observed again. This observation is made several times and than an algorithm calculates the position of the cameras and the screen. This is possible, because it is assumed that the screen and the cameras are already calibrated.
By observing the screen via a sphere on different positions, one can fix the positions of the cameras and the screen. Due to the fact that one knows the slope of the surface, one can reverse the measuring process and calculate not the slope of the specimen, but the position of the camera.

2.2.3 Results of the calibration

An example of a result of such a calibration is shown in tab. 2.1 and tab. 2.2.

Description	Focal Length [m]	Principal Point [m]		Decentring Distortion	
Parameter	c	xp	yp	p1	p2
Value	$6.203354 * 10^{-3}$	$-2.473 * 10^{-6}$	$-9.7105 * 10^{-5}$	$2.633 * 10^{-2}$	0.19649
Description	Radial Distortion			In Plane Distortion	
Parameter	k1	k2	k3	b1	b2
Value	5981.3	$-1.2355 * 10^{8}$	$-1.5379 * 10^{12}$	$1.6257 * 10^{-4}$	$-4.9851 * 10^{-5}$

Table 2.1: Example of a set of parameters used for internal calibration of a camera for a PMD setup. The distortion and positioning errors can be directly implemented into $softPMD$

zerobase	-0.63538	-1.50724	1.86423
xbase	0.98127	-0.10302	0.16277
ybase	0.18938	0.67058	-0.71725

Table 2.2: Example of a set of parameters used for external calibration of a camera for a PMD setup. Zerobase describes the distance between the origin of the coordinate system of the setup and the camera as a linear vector in meters. Xbase and ybase describe the angular orientation of the camera as Euler-vector.

2.2.4 Stereo deflectometry

Knowing the absolute position of the object, it is not sufficient to observe it with one single camera. With just one camera one can only know, that the object is on the line of sight of this camera, but not exactly where on this line. The situation is shown in fig. 2.9.

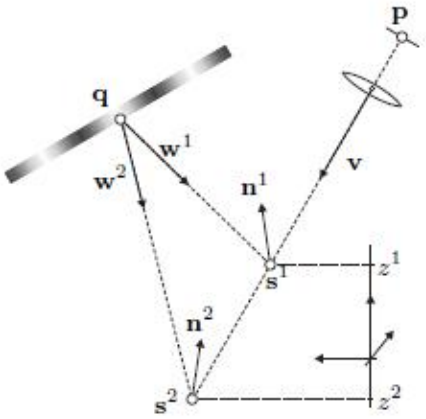

Figure 2.9: Scheme of the observation of an object with one camera via PMD. Even with knowing v and q it is not possible to distinguish between the object s^1 or s^2. Picture from [7]

To overcome this problem, one can install an additional camera. With two cameras observing the same point of the surface a second line of sight is added. The second line of sight gives the possibility to pinpoint the resulting normals and get a real position of the observed object. Of course this position is only theoretically perfectly determined. Due to the lateral and angular resolution of the setup, it is not possible to find exactly one possible normal fitting on both camera measurements. The best results of this stereo approach can be seen if the angle between the two lines of sight is close to 90 degree.

2.3 Reflectivity

Since the intensity of the emitted Cherenkov light is very faint, it is crucial to collect as much light as possible. For this reason the reflectivity of the mirrors has to be as high as possible and should extend 85% in a wavelength range from 300 nm to 600 nm.
To verify this value, a method was needed to measure the intensities of the light that hits the mirror and of the light that is reflected back. Two different approaches were investigated to measure this. On the one hand, the intensities were measured with a photodiode mounted on a linear table. This setup gives the possibility to scan through the spot of the light source and through the reflected PSF (see fig. 2.10). Due to the high homogeneity of the red LED used for the 2f-setup, this light source was used as well to build this setup.

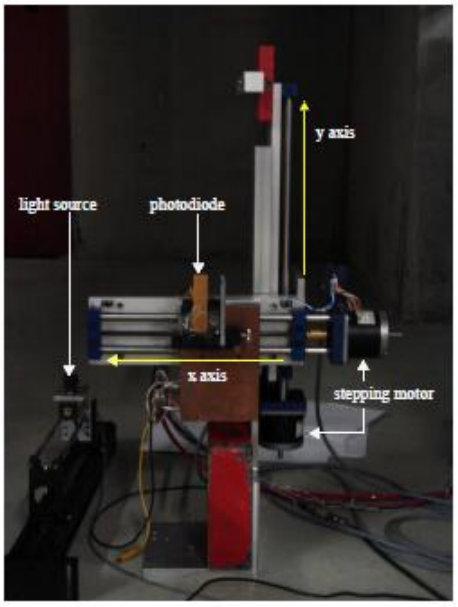

Figure 2.10: Setup used for scanning the PSF and the light emitted by the light source.

On the other hand, a setup was built using a CCD camera to observe the light. The principle layout of this setup is the same as for the 2f-setup, but both the PSF and the emitted light were observed with this camera.

2.4 Temperature behavior

To test if the optical properties of the mirrors are stable in a wide temperature range, tests in a climate chamber were needed. As the 2f-setup needs a lot of space and such a big climate chamber is not available, tests using this method could not be performed.
PMD has no such limitations as it is possible to construct a very compact setup that fits into a climate chamber. With this method, the PSF can be obtained under different temperature

conditions. A setup was built up and installed in an existing climate chamber at the facility of DESY in Zeuthen and first measurements were made.

2.5 Durability tests

The mirrors have to stand mechanical stresses like wind load, sandstorms and temperature changes without suffering damage. So the durability of the mirror tiles had to be tested as well. These tests were performed in Durham and are not part of this thesis.

Chapter 3

Measurements of PSF

3.1 Finding the position of the light source

Due to the fact that there are lenses in front of the LED the position of the LED and the (virtual) position of the real light source are different. To determine the focal length of the tested mirrors it is crucial to know the distance between the light source and the mirror very precisely. A technique is needed to figure out which is the real position of the light source. To find this position the mirror equation between the focal distance (f), the image distance (b) and the object distance (g) was used.

$$\frac{1}{f} = \frac{1}{b} + \frac{1}{g} \tag{3.1}$$

To get data for calculating the position of the light source in an easy way. It is helpful to have a test mirror with a small focal length. Performing the alignment of this setup is much easier, because the distance between the light source and the mirror is clearly reduced to one meter in contrast to 30 meter for the test mirrors. Such a mirror, available in Erlangen, is a HESS prototype with a nominal focal length of 641 mm. This mirror was positioned at different distances from the light source (g), and the PSF was searched and its minimum determined. The corresponding distance from the minimum PSF to the mirror was then the image distance (b).
To find the real position of the light source the equation (3.1) has to be altered to

$$\frac{1}{f} = \frac{1}{g+c} + \frac{1}{b} \tag{3.2}$$

with c as a correction of the measured object distance. After collecting data for several positions of the mirror, a fit can be performed to get values for c and f. All in all two fits were performed. First of all c and f were free to fit and in the second approach c was fixed at 0 and just f was free to fit. Both fits lead to reasonable results.

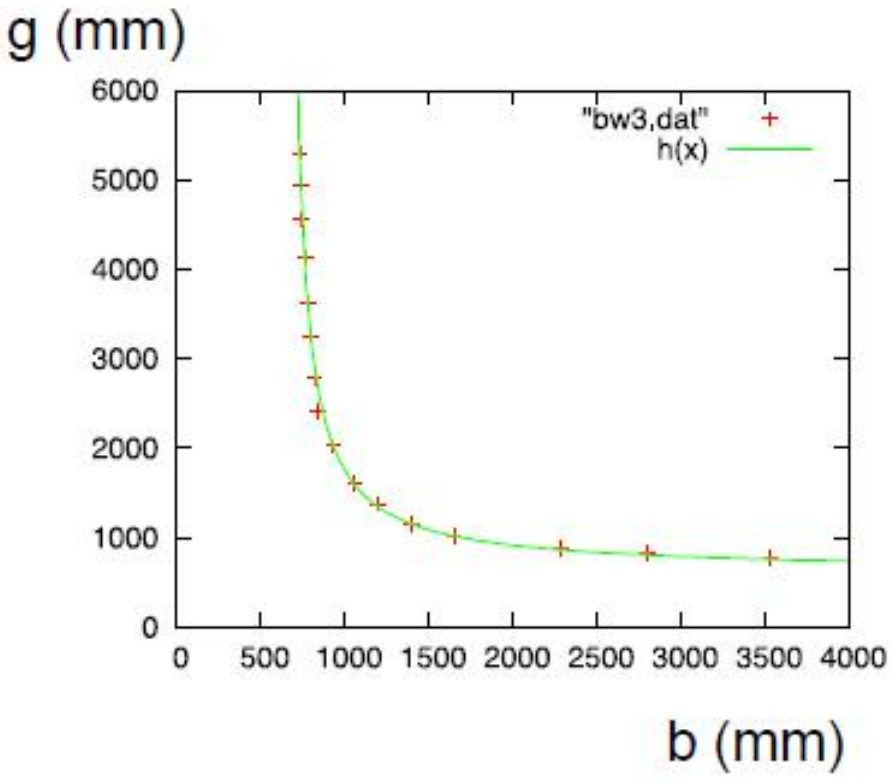

Figure 3.1: Result of the fit of the mirror equation with correction bias c.

In fig. 3.1 the fitting result is shown with the use of c. The result of this fit $f = (635.1 \pm 1.7)$ mm, $c = (-1.5 \pm 2.8)$ mm and $\chi^2 = 12.4$.
If c is fixed to 0 the result is $f = (636.0 \pm 0.4)$ mm and $\chi^2 = 12.4$. These results lead to the conclusion that the correction with c is not needed to find the real position of the light source. So the measured object distance is the real object distance that should be used for all calculations performed with the acquired data.

3.2 Measurements of the PSF with RGB-Camera

If you illuminate the mirror with the light source you will get the PSF on the screen. The PSF looks like in fig. 3.2 a. This particular PSF was taken from the HESS A153 mirror that was available in Erlangen for optical tests and measurements. The PSF was taken in the 2f-spot. Out of this picture you can determine the d80 value for this mirror by integrating over this picture.

3.2.1 Measurement results

The resulting jpeg picture was read in and converted into a *ROOT* file. A histogram was created out of the picture in that way, that no compression or rebinning was done to keep the resolution of the CCD picture.
To get rid of some background effects occurring due to the measurement conditions in the basement, a background picture was taken as well and subtracted from the PSF picture. This was done by reading in the background picture into *ROOT* and calculating the mean value of the background. This mean value was then subtracted from every single pixel of the PSF histogram. The resulting picture was then analyzed.
To determine the d80 value it is necessary to know the 100% intensity. This was found by integrating over the whole picture. After that the center of gravity of the picture was searched and, starting from this point, a circular integration with increasing radius was performed. The radius was increased in steps. If the integration over the resulting circle lead to an intensity lower than 80% of the whole picture intensity the radius increased again. At 80% intensity the integration stopped and the diameter of the resulting circle was taken as d80 value. A resulting picture is shown in fig. 3.2 b.

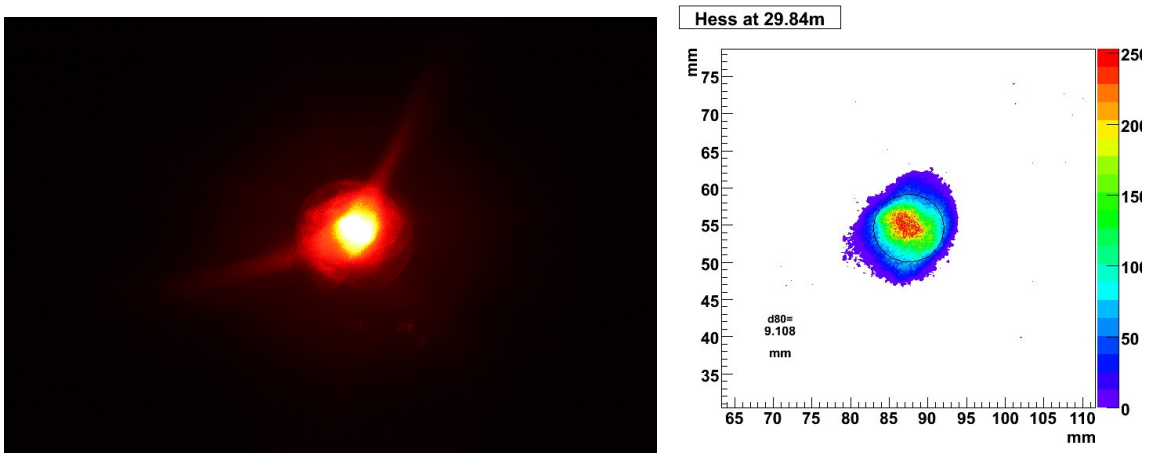

(a) Original picture from the CCD camera

(b) Analyzed picture after background subtraction. The circle marks the d80 value.

Figure 3.2: PSF taken from a HESS mirror at 2f distance and analyzed with *ROOT*.

3.3 Measurement with PMD

PMD as a deflectometric technique can not directly observe the PSF of a mirror. It was developed to observe specular free form surfaces and out of the results of this observation the PSF can be calculated.

3.3.1 Measurement results

Out of a single PMD measurement, different types of data can be accomplished. The prime measurand was the slope of the mirror in x- and y-direction. So a map of the surface for the slope in x and y-direction could be obtained. Via integrating the slope the normals and the surface-shape of the object could be calculated. By differentiation a local curvature map was created. A collection of the different result types can be found in fig. 3.3.

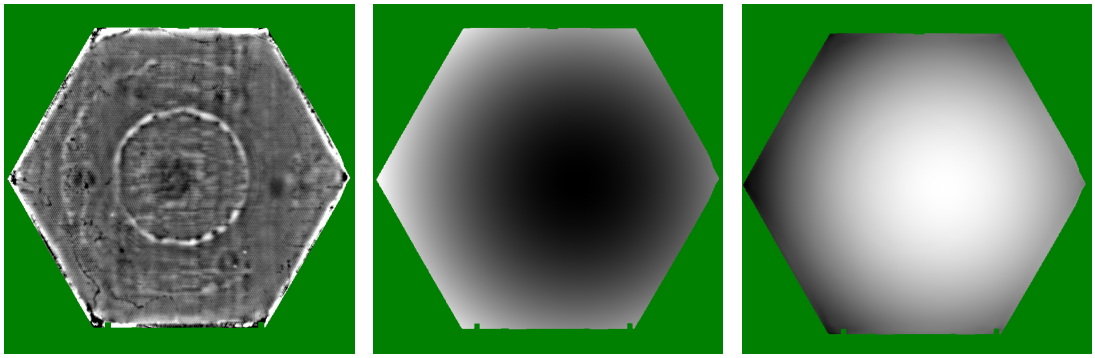

(a) Curvature map (b) Surface map (c) Normals

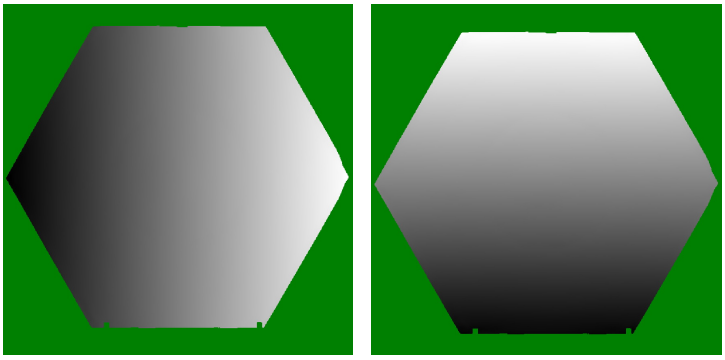

(d) Slope in x-direction (e) Slope in y-direction

Figure 3.3: Results of a PMD measurement from a LST prototype from Japan.

The results shown in fig. 3.3 are overlayed by the tilt of the mirror. The slope of the mirror is mainly induced by the global slope or tilt of the mirror in space and not by the mirror itself. To overcome this effect, the maps were projected on a plane. So the tilt was neglected and the intrinsic properties of the mirror itself could be observed. The local curvature was not effected by this so there was no need to project the curvature map. This lead to the four changed maps in fig. 3.4.

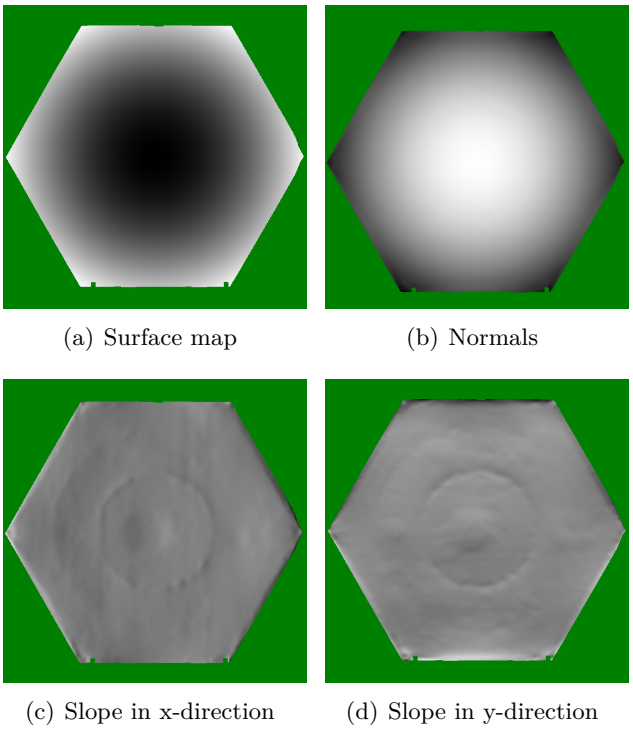

(a) Surface map (b) Normals

(c) Slope in x-direction (d) Slope in y-direction

Figure 3.4: Results of a PMD measurement after projecting on a plane from a LST prototype from Japan.

After getting rid of the global tilt of the mirror itself, much more intrinsic structures could be seen. Especially in the slope maps structures were recognizable. The example in fig. 3.4 shows a ring structure in the middle of the mirror and some small structures surrounding the inner ring. The same structures are already visible in the curvature map in fig. 3.3.
The surface map was still overlayed by a global structure. The mirrors were constructed to focus the light hitting the mirror. So the mirror was as part of a sphere curved. This curving could be seen in the surface map. To make imperfections of the surface visible there was the possibility to substract a sphere from the surface data to see the deviations of the surface from the perfect sphere. This was done in fig. 3.5. The same structures are visible like on the slope and curvature map, but some deviations can also be seen in the corners of the mirror.

All the different types of results show different properties of the mirror. For industrial development of the mirrors the curvature map is useful. One can see small structures on the surface and can find out what has to be changed in the production process of the mirror to improve it.

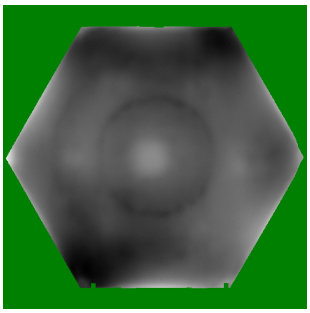

Figure 3.5: Result of a PMD measurement. Surface map after projecting on a plane and substracting a sphere to visualize deviations from the perfect sphere of the surface. Picture from a LST prototype from Japan

To verify the optical properties of the mirror, the d80-value is needed. The PSF is simulated out of the shape and the normals of the mirror via raytracing. Out of this PSF, the d80 could be determined in a similar way as it was done for the 2f-measurement.
With PMD measurements, one can get a full set of data to characterize the most critical properties of a mirror. Up to now, the only optical property that could not be measured within a PMD-setup is the reflectivity of the mirror.

3.3.2 Raytracing

With raytracing a reflection process is simulated. The general idea is to simulate the real situation on the telescope. A light distribution is simulated with its origin in infinity. An infinitely far away light source means that all rays of light are parallel to each other. This parallel light is now focused by the mirror in the focal point. With raytracing it is possible to simulate the real behavior of the mirror on the telescope itself. The real focused spot and its size can be determined. A sketch of this raytracing can be seen in fig. 3.6.

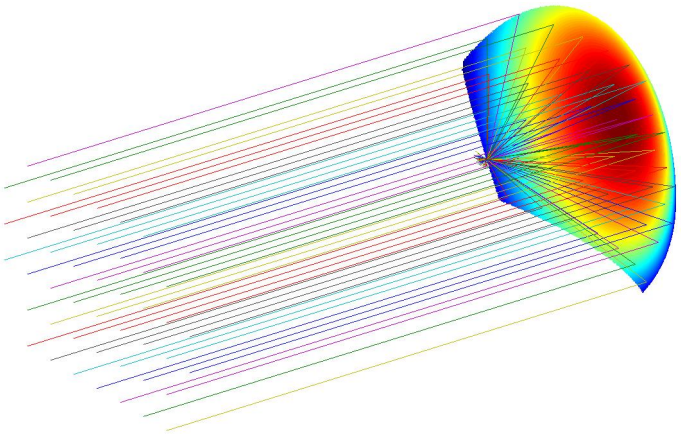

Figure 3.6: Sketch of the raytracing process for a spherical mirror and parallel light coming from infinity.

To make this raytracing result more comparable to results obtained with the classical 2f-measurement the simulated light source was changed. A perfectly point-like light source emitted a certain number of rays, which pointed on the mirror surface. The reflection of the rays on the surface was simulated with the help of the normals and surface data obtained with PMD. These reflected rays were finally collected and visualized, so that the resulting PSF was visible. For a perfect mirror and a perfect light source the resulting raytraced PSF would be a perfect point. As the mirror is not perfect and its imperfections are measured within the shape and the normals data from PMD, the resulting PSF will not be point-like but spread out. A raytracing function is in the literal sense a point spread function because it spreads a point-like source with the help of an imperfect surface.

3.4 Comparison of the both techniques

Both techniques, 2f-PSF and PMD, were used in parallel to observe the same mirror. Out of the spatially resolved data from PMD the PSF was raytraced. This gave the possibility to compare both results. The measurements of PMD were performed with the so called long working distance (LWD) setup. This setup was constructed to measure mirror prototypes in a similar way as in the classical 2f-way. The mirror was observed by two cameras and illuminated by a relatively small screen. As the LWD-setup is using an extended light source it is not needed to position the setup directly in the 2f-point, but near by. This made the alignment of the mirror and the setup easier than at the 2f-setup, but one needs as well a long and dark corridor for measurements.

Figure 3.7: LWD-setup used in Erlangen to perform comparing measurements with classical 2f-measurements

The LWD-setup has two cameras, what makes in general stereoscopy possible. But to the fact that the distance between the mirror and the setup was at least 30 m, the angle of the lines of sight of the two cameras were close to zero degree. This means that stereoscopy was impossible. To get the exact position anyway the distance had to be measured with an external device. For this purpose a Bosch distance meter was used.
The comparison was done with respect to two properties of the results. First of all it was checked if the shape of the PSF fits or not. The second property to test was the size of the d80 circle for different distances from the mirror to the screen.
As it can be see in fig. 3.8 the shapes of the PSFs for both methods were differing. The raytraced PSF looked much more resolved, as one can see fine structures within the PSF that can not be seen in the CCD-picture. To overcome this problem different tests were performed and led to the conclusion that the main reason for this discrepancies is the extension of the real light source.
The raytracing procedure simulates a perfect point-like light source. Out of this light source the rays are traced to the mirror, reflected on its surface and traced back to a certain point. If this point has a distance to the mirror close to its radius of curvature, the resulting picture will be the PSF of this mirror.
For the classical 2f-method a real light source was used. This light source will never be perfectly point-like. If you observe the PSF that comes from a mirror that is illuminated by a not point-like light source, the PSF will be smeared. That is the effect that can be seen in fig 3.8.The shape of the PSF is smeared in the 2f-picture and the value for d80 shows a big diference in comparison of the two methods.

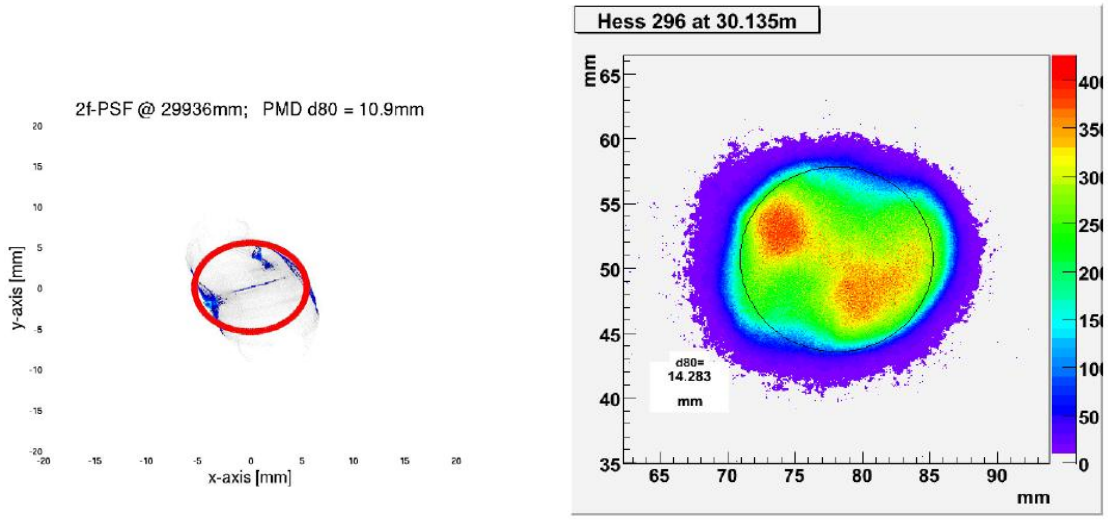

(a) Raytraced PSF from a PMD measurement. The red circle shows the d80.

(b) PSF taken by a CCD camera and analyzed with *ROOT*. The black circle shows the d80 value.

Figure 3.8: PSF of the HESS A296 mirror.

To overcome this effect, a convolution of the simulated light source was performed. The function of the point-like light source was convolved with a Gaussian profile with a certain

σ. This σ is a direct expression for the extension of the light source. The σ of a Gaussian profile describes the total width of the function and so in this case the total width of the light source.
By performing this convolution for different sigmas and different distances, fig. 3.9 was produced. One can see clearly that the shapes of the PSFs are drastically changing by introducing such a σ. The smearing effect is getting stronger if the σ-value is rising. It can be seen as well that the PSF is not just smeared in the focal spot, but for all positions.

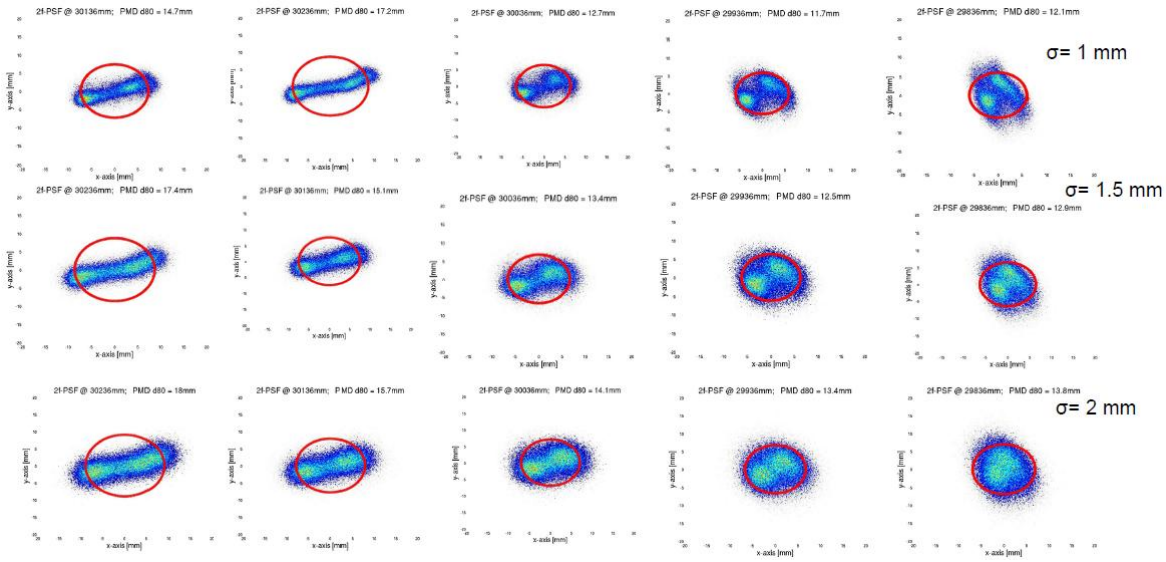

Figure 3.9: PSFs of the HESS A296 mirror after convolving the light source used for raytracing at different positions and with different σ. The red circles show the d80.

Taking a closer look at these convolved PSFs shows that the shape is now comparable to the 2f-shape. The best fitting shapes can be seen in fig. 3.10. The difference in the d80 value is now smaller and the shape fits better than by using the raytraced PSF without convolving. There is still a difference in the distance caused by problems in the raytracing routine. To overcome this discrepancy further studies are needed.

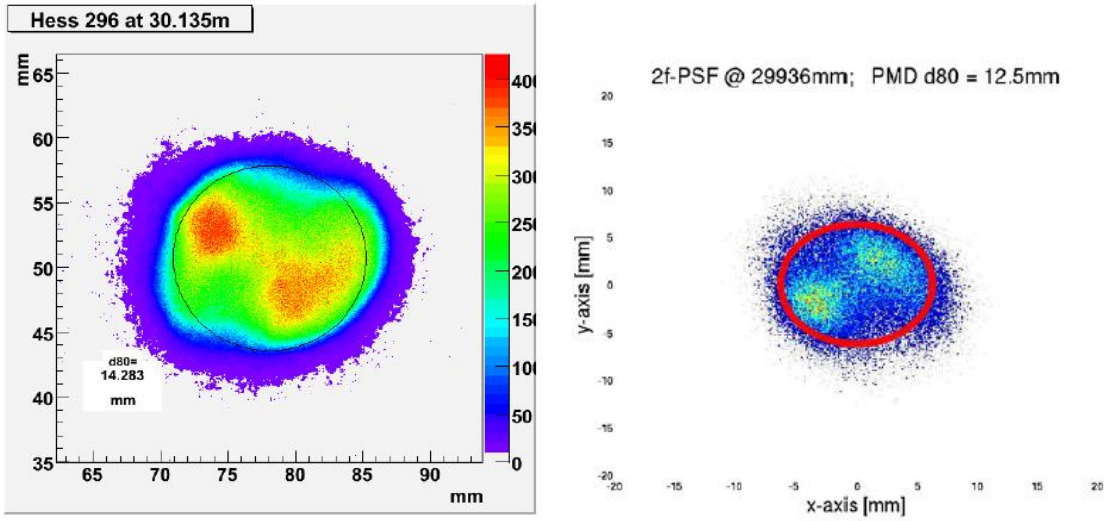

(a) 2f-result analyzed with *ROOT*. The black circle shows the d80.

(b) Convolved raytracing result with a σ of 1.5. The red circle shows the d80 value

Figure 3.10: Comparison of the results of PMD and 2f-measurement of the mirror HESS A296.

Comparing the d80-values of convolved raytracing and real measurement, one can still see a difference between both methods. Though the difference is decreased after convolving the light source there are still some differences remaining.
In fig. 3.11 is shown that the matching of the shapes of the PSFs of the mirror HESS A153 is better than for HESS A296. But also on this mirror some differences are remaining.

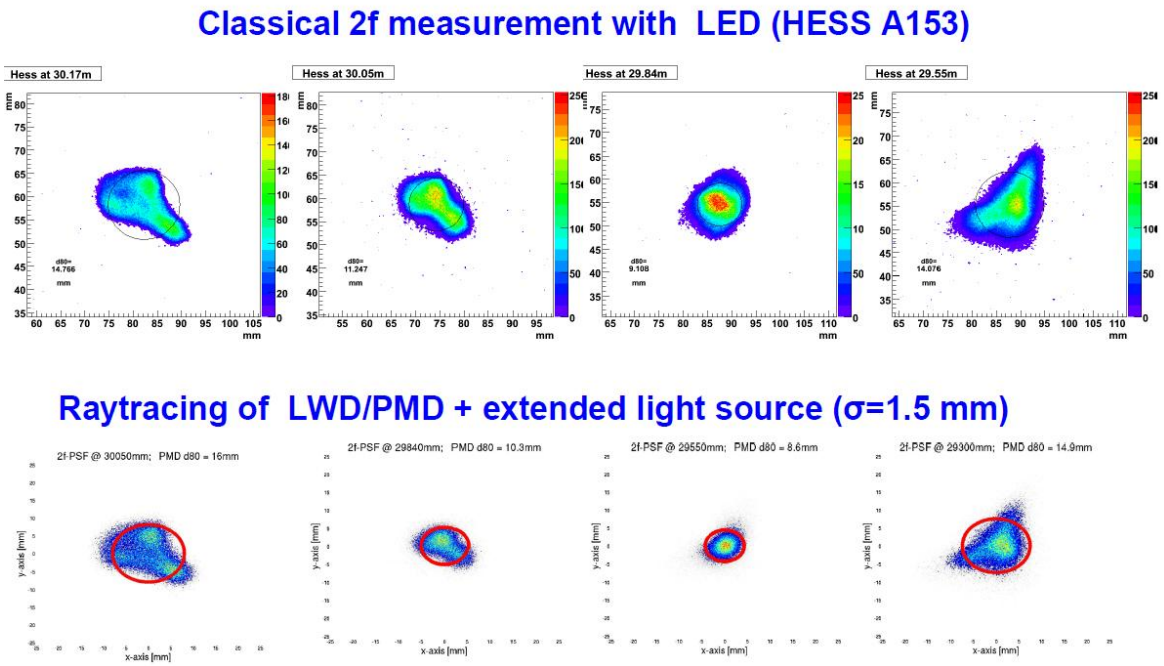

Figure 3.11: PSFs of the mirror HESS A153 after convolving the light source used for raytracing at different positions and a σ of 1.5 mm. The circles show the d80.

In the focal spot the PSF is nearly the same for both methods. But even further away from the focal spot, where the PSF is more structured, the shapes are fitting nearly perfectly (see fig. 3.12).

An explanation for these differences would be the fact, that raytracing simulates a perfect

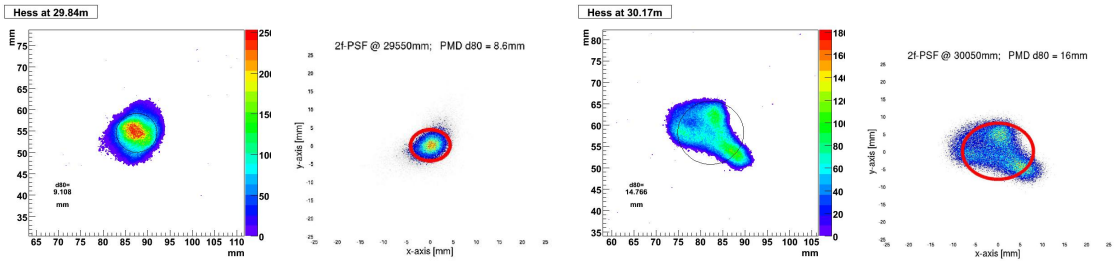

(a) Result of a 2f-measurement in the focal spot analyzed with *ROOT*. The black circle shows the d80.

(b) Convolved raytracing result with a σ of 1.5 mm in the focal spot. The red circle shows the d80

(c) Result of a 2f-measurement out of focus analyzed with *ROOT*. The black circle shows the d80.

(d) Convolved raytracing result with a σ of 1.5 mm out of focus. The red circle shows the d80

Figure 3.12: Comparison of the results of PMD and 2f-measurement of the mirror HESS A296.

camera to observe the PSF. But in reality there is a ground glass in front of the camera and the camera itself has some optical components like lenses in the objective. These additional

optical layers introduce distortions, stray light and other effects that change the picture of the PSF. Since these effects were hard to handle and not completely understood, a simulation of them was not introduced into the raytracing procedure.
Raytracing simulates not only a perfect camera, but a perfect light source as well. Even after convolving the light source, the light distribution is homogeneously spread over a certain angle. This means that all parts of the simulated mirror are hit by the same intensity of light. For the real measurements this is not the case. Even if the used light source has intensity fluctuations of about only 2%, this influences the results.

3.5 Round-robin test

To show and compare the different testing methods available throughout the mirror work package, a round-robin test was initiated. This test included the testing of three different types of mirrors in every institute that was willing to provide optical tests for the CTA mirrors. These three mirrors were the previously shown HESS-I mirror (A296), a MAGIC-mirror (901) and a CTA prototype from Saclay (25). Every mirror was produced with a different technique. The HESS mirror is a massive polished glass mirror, the MAGIC mirror is a diamond milled composite mirror and the Saclay prototype is a cold slumped composite mirror. This gives the opportunity to see if the testing methods can give comparable results for different mirror techniques. The size of the PSF is mainly caused by the shape deviation from a perfect sphere. If the mirror was a perfect sphere the PSF would be a point or as large as the light source. By imperfections in this sphere the point of the point-like light source is spread. This defines the PSF of the mirror.
In Erlangen both the 2f-measurement and a PMD measurement of every single mirror were performed. The accomplished data was analyzed as described earlier.

3.5.1 HESS A296

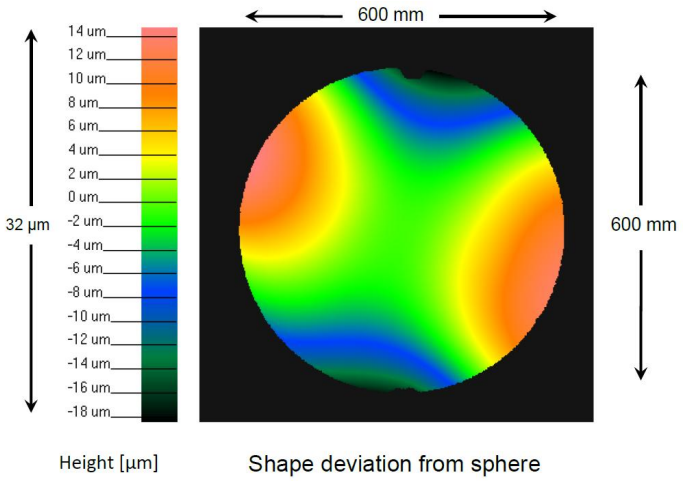

Figure 3.13: Shape deviation from a perfect sphere of the mirror HESS A296.

The HESS mirror is a massive polished glass mirror of the same type like the HESS A153 that was used to build up and test the setup and analyzing routine. The mirror is circular with a diameter of 60 cm. For this mirror the same behavior was expected as found for HESS A153. So the raytraced PSF was convolved and compared with the PSF obtained with the CCD camera (see fig. 3.14).

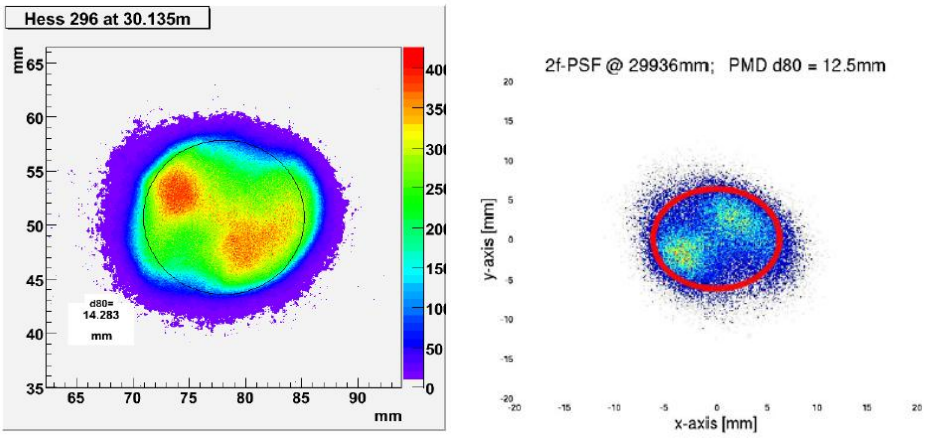

(a) 2f-result analyzed with *ROOT*. The black circle shows the d80.

(b) Convolved raytracing result with a σ of 1.5 mm. The red circle shows the d80.

Figure 3.14: Comparison of the results of 2f- and PMD-measurement of the mirror HESS A296.

These results show very nice agreement in shape and size of the d80. The difference in the focal length is still existent and the orientation of the raytraced PSF is different than the one

from the CCD camera. These two effects are supposed to be caused by software problems in the raytracing routine.

3.5.2 MAGIC-901

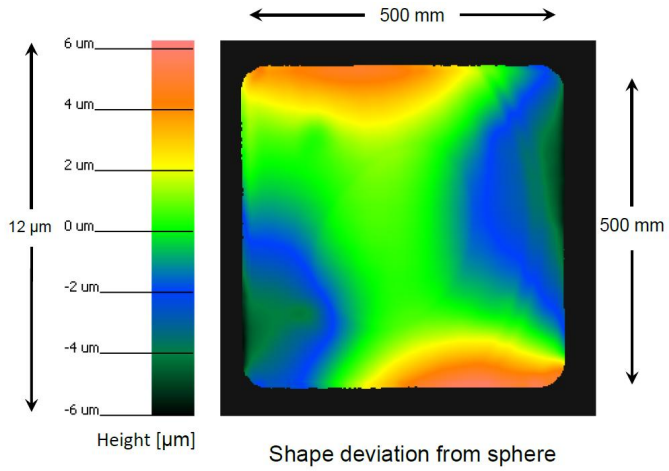

Figure 3.15: Shape deviation from a perfect sphere of the mirror MAGIC 901.

The mirror MAGIC-901 was produced for the MAGIC telescope on La Palma and is a composite mirror with diamond milled surface. The mirror has a rectangular shape of 50 cm by 50 cm. The measuring results for this mirror can be seen in fig. 3.16.

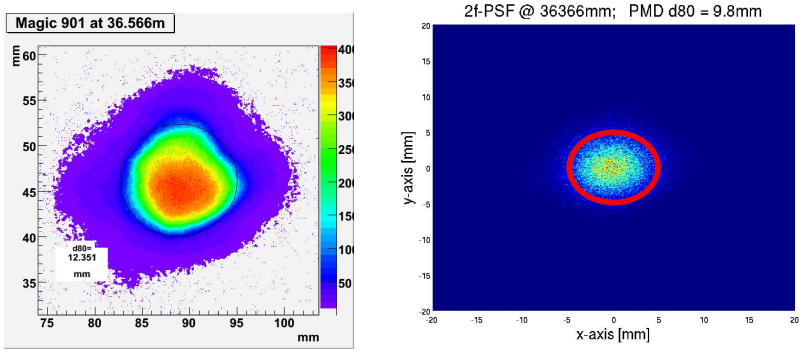

(a) 2f-result analyzed with *ROOT*. The black circle shows the d80.

(b) Convolved raytracing result with a σ of 2 mm. The red circle shows the d80.

Figure 3.16: Comparison of the results of2f- and PMD-measurement of the mirror MAGIC 901.

For this mirror the difference between the raytraced and the 2f-PSF is greater than for the HESS mirrors. This can be explained with the micro-roughness of the surface for this particular mirror type, that is introduced by the diamond milling technique. The size of this structures is much smaller than the lateral resolution of PMD, so these structures can not be

resolved. These small structures on the reflective surface of these mirrors introduce diffuse reflections and stray light that widens up the PSF of these mirrors. Since the surface used for raytracing is free from this micro-roughness, these effects are completely neglected. This changes the PSF coming out of the raytracing routine with respect to the real PSF observed by the CCD camera.

3.5.3 Saclay 25

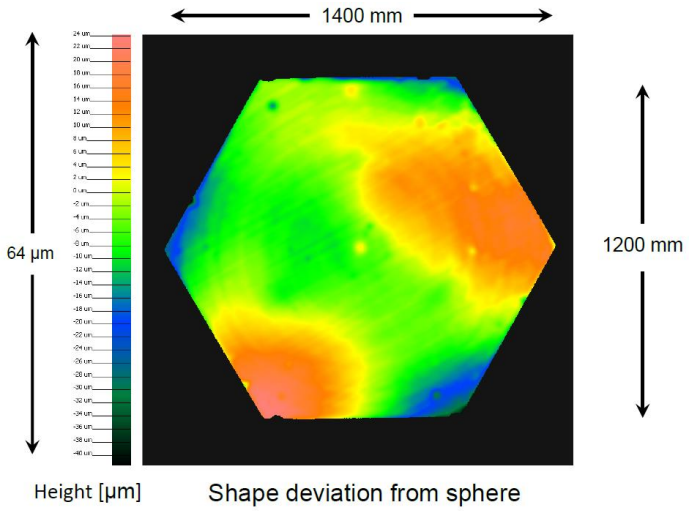

Figure 3.17: Shape deviation from a perfect sphere of the mirrorSaclay 25.

The mirror from Saclay is a CTA MST prototype with hexagonal shape and a size of 1.20 m flat-to-flat. The mirror is a cold slumped composite mirror and its measuring results can be seen in fig. 3.18.

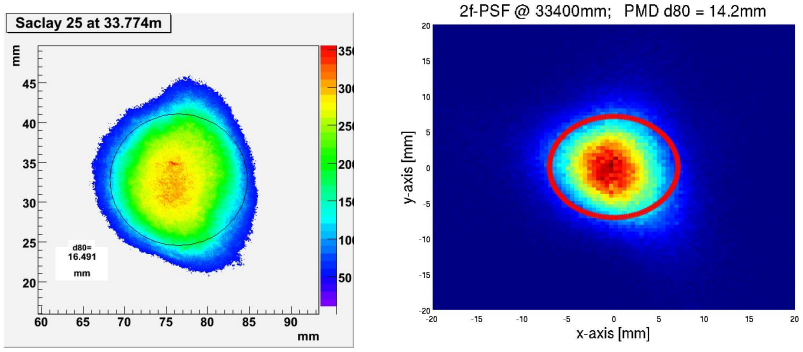

(a) 2f-result analyzed with *ROOT*. The black circle shows the d80.

(b) Convolved raytracing result with a σ of 2 mm. The red circle shows the d80.

Figure 3.18: Comparison of the results of 2f- and PMD-measurement of the mirror Saclay 25.

This mirror has no micro-roughness because this effect is not occurring with the cold slumping technique. Therefore the results of both measuring methods are matching.

A collection of all the results for these three mirrors can be seen in tab. 3.1. The value for shape deviation is a peak to valley value and can be seen in figs. 3.13, 3.15 and 3.17.

Mirror	Shape deviation	d80-PMD (convolved)	d80-2f
Saclay 25	64 μm	14.2 mm	16.5 mm
HESS A296	32 μm	12.5 mm	14.3 mm
MAGIC 901	12 μm	9.8 mm	12.3 mm

Table 3.1: Collection of the results for the mirrors tested in the round-robin campaign.

The results of both used methods to measure the mirrors are matching nicely. The still existing differences in the d80 values can be explained with micro-roughness of the surface of the mirror, especially the MAGIC mirror and optical distortions introduced by the CCD camera and the ground glass.

Chapter 4

Measuring the PSF in a climate chamber

Even though the decision where CTA will be build is not made yet some features of the site are clear due to the needs of such a big telescope array. First of all it will be on the southern hemisphere to get the possibility to observe the galactic disc, especially the galactic center. The next settlement should be quite far away from the telescopes to get rid of stray light in the atmosphere coming from street lamps or other anthropogenic light sources. The weather conditions shall be arid with many clear nights to have as much observation time as possible. Not many of such places are still existing around the world. This leads to the point that the most probable site location will be in a desert or desert-like environment. In such environments the temperature will increase extremely during the day and drop drastically during the night. The optical properties of the mirrors have to be stable over the full range of temperature they will experience. So the requirements for the mirrors say, that the PSF has to stay in the in chapter 1.2.2 given restrictions, for temperatures between $-10°C$ and $+30°C$.
To check if the prototypes fulfill these requirements some tests in a climate chamber are necessary. Available techniques to measure the PSF of mirrors (2f-method and PMD using the LWD-setup) need a long distance to observe the mirror. A room of such a length of about 30 m for MST or even nearly 60 m for LST mirrors can not be air-conditioned in a proper way. To make such measurements possible anyway, the PMD setup was altered to a so called short working distance (SWD) setup. This setup has such a small footprint, that the existing climate chamber at DESY Zeuthen (size of 4 m by 6 m) could be used. This lead to the possibility to observe the behavior of the mirrors at different temperatures.

4.1 Design of the SWD-PMD-setup

The SWD-setup was designed in Erlangen with the goal to get a compact setup that would fit into the existing climate chamber at DESY Zeuthen. A technical drawing of this setup is shown in fig. 4.1.

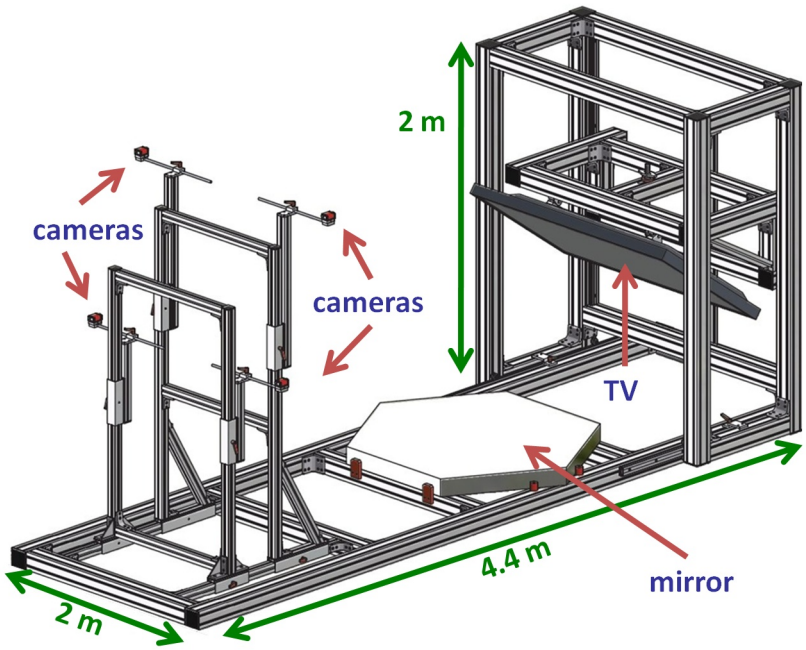

Figure 4.1: Technical drawing of the short working distance setup including four cameras and a 60" screen.

For this setup it is necessary to have four cameras, as it is not possible to observe the whole mirror with just one camera. To see the field of view of the single cameras see fig. 4.2

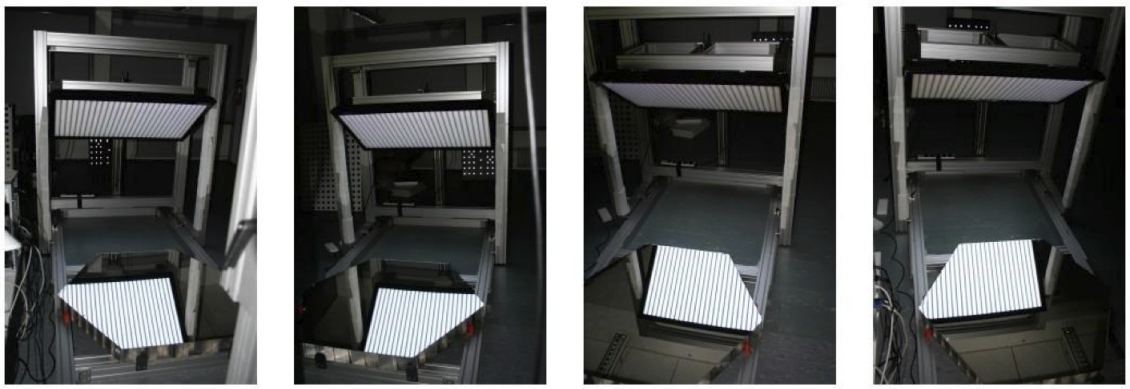

Figure 4.2: View of the four cameras of the SWD-setup on the mirror. Every camera observes more than one quarter of the mirror.

An overlap area of the observed part of the mirror between all four cameras exists. This allows to perform stereo measurements and gives the opportunity to calculate the distance

between the mirror and the cameras. So there is no need to measure these distances as it was for the LWD-setup. A visualization of this overlap regions can be seen in fig. 4.7.
The setup was build up in Erlangen to test its functionality. Afterwards it was disassembled and shipped to Zeuthen where it was rebuilt in the climate chamber (see fig. 4.3).

(a) The screen mounted in its holder.

(b) The four cameras.

Figure 4.3: SWD-Setup in the climate chamber in Zeuthen.

4.2 Calibration in the climate chamber

4.2.1 First approach

The SWD-setup in the climate chamber had to be calibrated as well. Two calibration steps, internally and externally, had to be performed. For this purpose a calibration plate was designed. As in Erlangen, a poster with black dots on white ground was used to internally calibrate the cameras. For external calibration of the whole setup a HESS-I mirror with very good optical properties was used. One can assume it is part of a perfect sphere without doing a big error.
The necessity of using four cameras leads to another problem. In general one can say that there are four measurements performed in parallel. Every single camera can be seen as a single measurement. To get a full field measurement of the mirror tile, one has to combine these single measurements. For this purpose the external calibration of the setup is crucial. The positions of the cameras to each other had to be known very precisely.

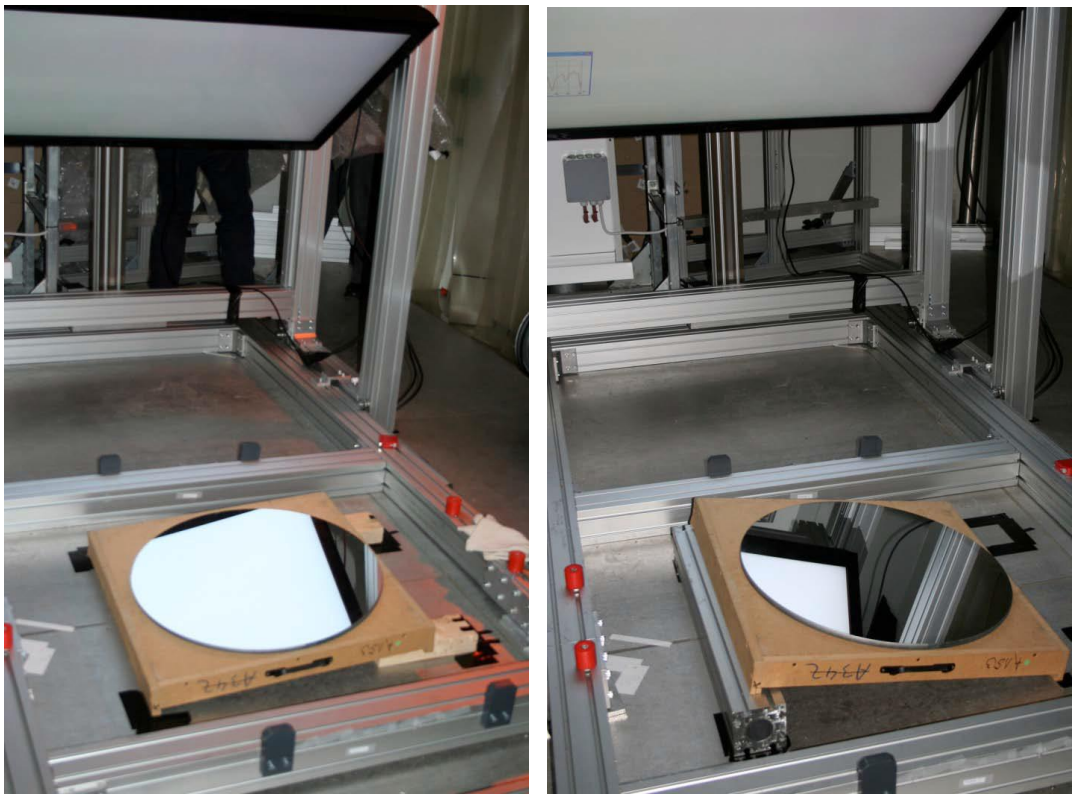

(a) Calibration with 5° tilt.

(b) Calibration with 10° tilt.

Figure 4.4: Calibration approach with a HESS-I mirror.

The calibration routine was performed in the way that the mirror was placed in the middle of the setup and positioned in several orientations. For every single orientation a measurement was taken with all four cameras. Out of these pictures the positions of the cameras were calculated as described earlier. It can be seen in fig. 4.4 that the mounting of the HESS mirror was an ad hoc solution and not well equipped. This reduced the reliability and the repeatability of the whole routine.
After the measurement the data was analyzed for every camera separately. Afterwards the results had to be combined. A very first combination of measurements is shown in fig. 4.5.

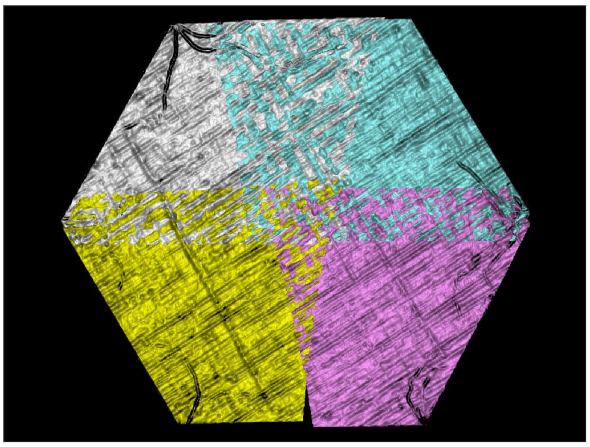

Figure 4.5: Very first combination of the curvature results of the four cameras for the climate chamber measurement of the Saclay-prototype #13. Different colors show different cameras.

As one can see, the patching of the different camera images does not fit. There is a gap on the lower edge and the left and right corners are not exactly overlayed by the two cameras. That means, that the calibration of the setup was not sufficiently precise. The algorithm for searching the positions of the cameras came to a result that is not exactly the truth. So the pictures of the single camera measurements are shifted.
Consequently it was necessary to improve the calibration routine.

4.2.2 Improvements of the calibration

Improvement of the internal calibration

The internal calibration routine was improved in several ways: First of all the dotted poster was changed. Now there is a poster with white dots on black background. This way of marking is much more stable and *australis* can find the marks more precisely.
The fixation of the dotted poster was also improved. The poster was not just fixed on a simple poster wall but glued on a dummy-mirror existing in Zeuthen (see fig. 4.6). These dummies are curved metal plate which have exactly the shape of a MST mirror tile and were produced to be mounted on a quarter-dish prototype in Zeuthen. A spare one could be used as fixation base.
The third improvement was the implementation of a hexapod in the setup. In this way positioning of the dotted plate was much easier, precise and repeatable. An other advantage of the hexapod was that the positioning of the dotted plate could be done from outside the climate chamber. No one had to enter the climate chamber under inconvenient conditions and the doors of the chamber could stay closed as long as possible to avoid disturbances of the temperature and humidity inside the chamber.

Improvement of the external calibration

The external calibration was improved as well. First step of improvement was to change the calibration mirror from a HESS-I mirror to a HESS-II mirror, so a change from a circular mirror with 60 cm diameter to a hexagonal mirror with 90 cm flat-to-flat. This means to use a bigger part of a perfect sphere to figure out the positions of the cameras. This makes the algorithm much more stable and leads to a more precise result (see fig. 4.6).

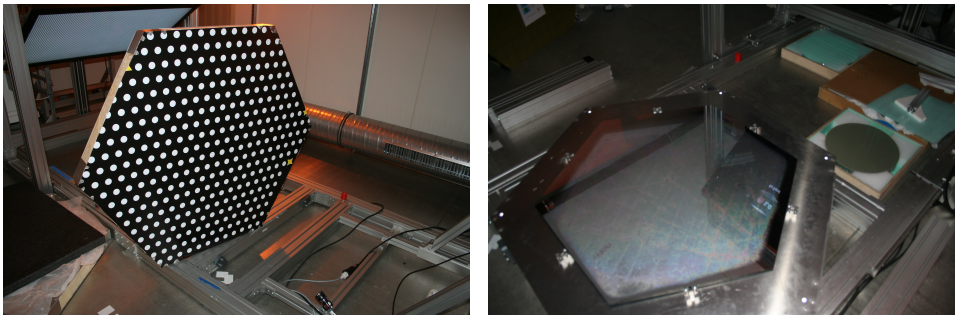

(a) Improved target for internal calibration. (b) HESS-II mirror as calibration target for external calibration on its holder.

Figure 4.6: Improvements of the calibration for the SWD-PMD in the climate chamber in Zeuthen.

The second improvement was to not just tilt the mirror in the center of the setup but to shift the mirror inside the setup. This introduces as well a translation of the perfect sphere and brings more variation into the algorithm used to find the positions. This as well leads to a much better result.

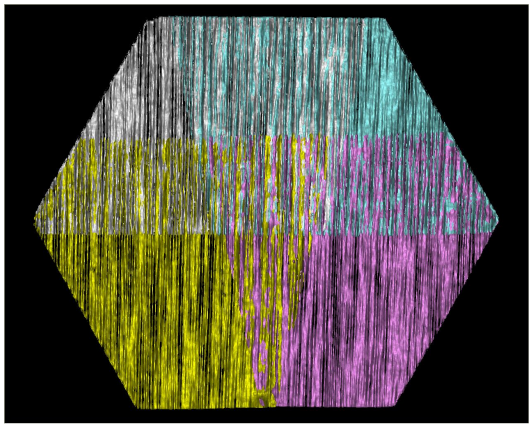

Figure 4.7: Combination of the curvature results of the four cameras for the climate chamber measurement of Saclay-prototype #9. Different colors show different cameras.

After the new calibration routine was performed the images of the four cameras are fitting much better than in fig. 4.5. There is no gap between the lower cameras and the corners are overlayed nearly precisely.

4.3 Results of the temperature dependence of the mirrors

After improving the calibration routine, an open issue was to find a prove if this improvements are really leading to more reliable results. It is expected, that for a massive glass mirror the focal distance should not change by temperature changing. As the HESS mirrors are massive glass mirrors and were used for calibration of the setup they were available in Zeuthen anyway. An additional measurement was introduced to check the focal distance of these massive glass mirrors. The results are shown in fig. 4.8.

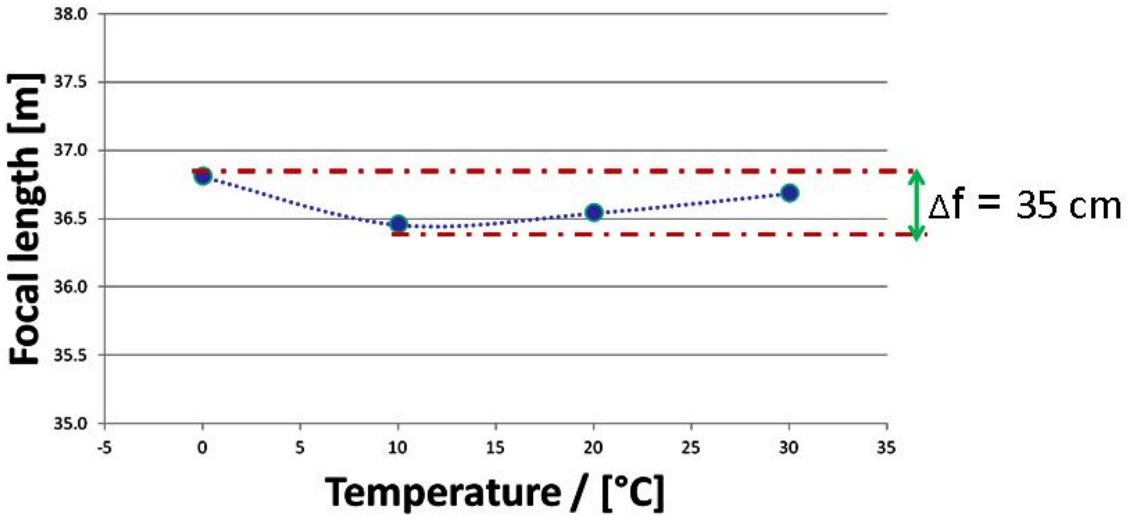

Figure 4.8: Temperature behavior of the focal length of a HESS-II mirror measured at different temperature steps.

The focal distance for this mirror is varying about 35 cm. This means $\frac{\Delta F}{F} \leq 1\%$. This error can be seen as very small. So the focal distance can be treated as constant over this 30°C range. This is accepted as a prove that the new calibration routine is more stable and reliable than before. This is also true for the gained results out of the new measurements.
As said before the most interesting value for these measurements is the focal distance of the tested mirrors. To get this value the mean curvature of the mirror is inverted. But this routine is not as exact as it should be to get reliable results. So raytracing was introduced into the climate chamber measurements.
Raytracing is a possibility to get the PSF of a mirror without the need of a very long testing room. But raytracing is not necessarily limited to the focal point of a mirror. The PSF can also be calculated at different distances. A possible method to get the focal distance out

of this is to raytrace the PSF on different positions and calculate the d80 value out of the different pictures. The position where the d80 value is smallest defines the focal distance. This was done for the tested mirrors in the climate chamber and is shown in example for saclay prototype number 9 in fig. 4.9.

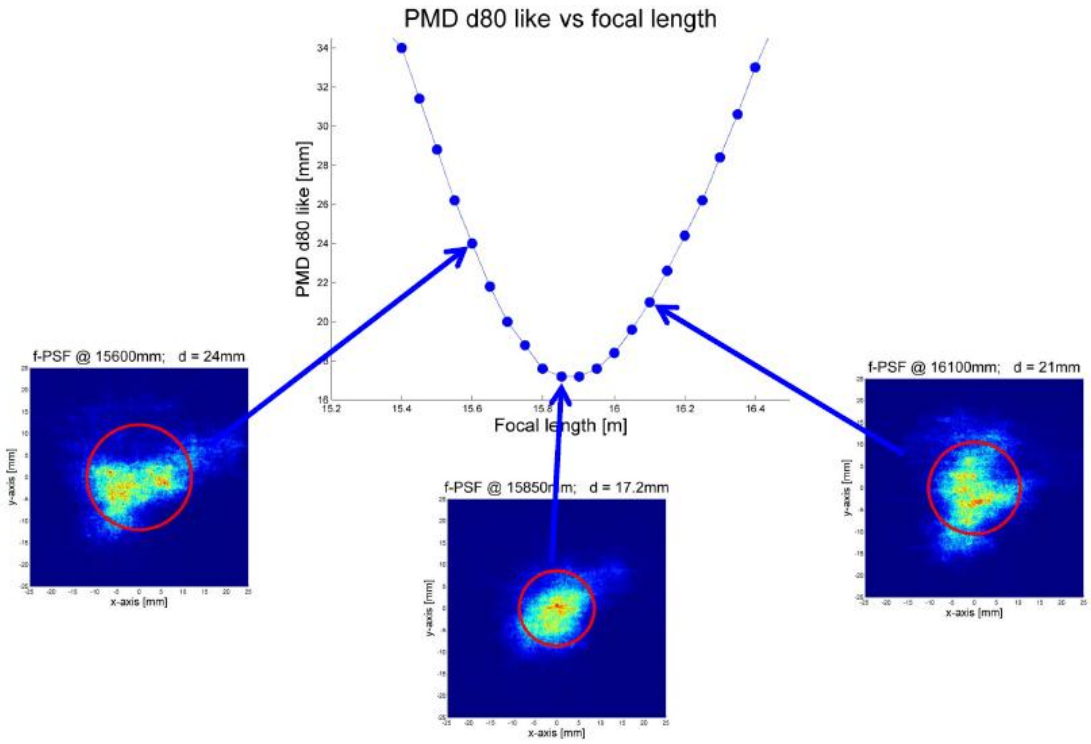

Figure 4.9: Example of a raytracing result for a climate chamber measurement at 30°C. All dots show a raytraced position. The line shows a parabolic fit on the data points. Three pictures of the raytraced picture at different positions are shown exemplary.

The same procedure can be done for all measured temperatures in the climate chamber and the results can be compared to see if the focal distance of the mirrors is changing due to temperature changes. This was also done for the mirror shown in fig. 4.9.

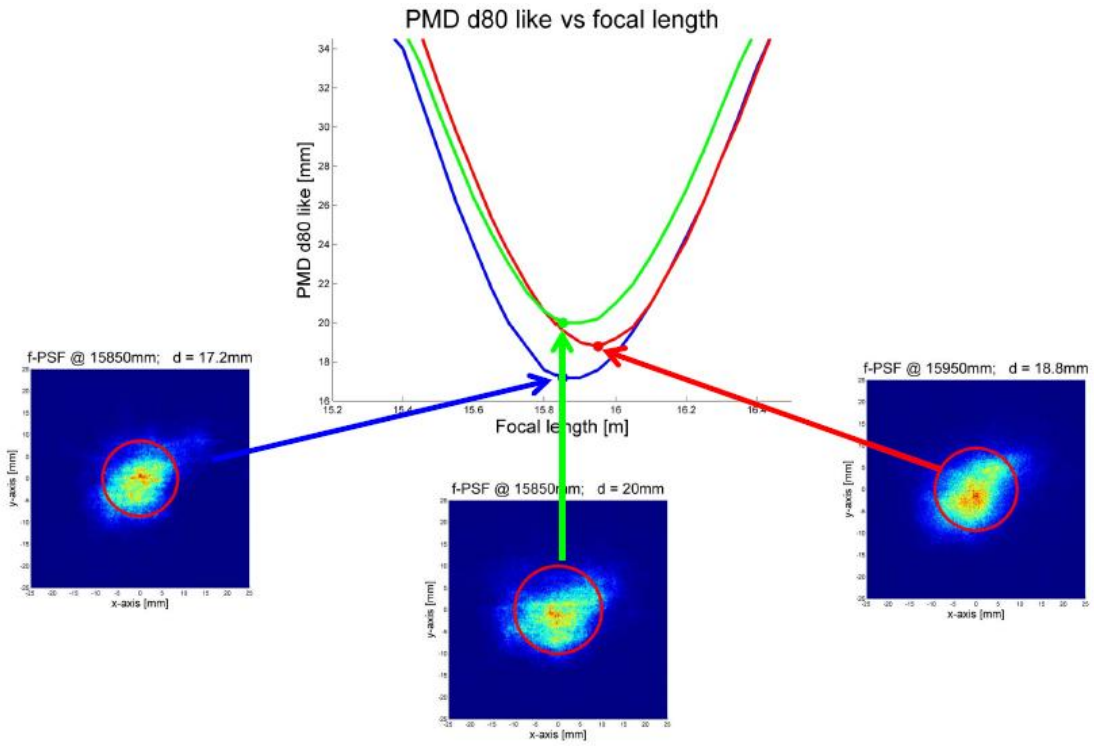

Figure 4.10: Example of a raytracing results for climate chamber measurements at different temperatures. The blue line shows the behavior at 30°C, green at 10°C and red at 0°C. Three pictures of the raytraced picture at the focal point for the different temperatures are shown.

One can see in fig. 4.10 the change of the focal distance of this mirror. The focal length seems to be stable between 30°C and 10°C and is increasing if temperature drops to 0°C. Out of three data points no behavior parametrization can be done. More data points are needed to systematically examine the temperature behavior of the mirrors.
Out of the plot in fig. 4.10 one can as well observe the behavior of the d80-value. This value seems to increase by lowering the temperature and decrease again at 0°C. For this value are also only three data points available, so the behavior can not be verified.

Chapter 5

Reflectivity

The reflectivity of the mirrors can be measured in two different ways. First of all one can measure the reflectivity directly at the surface of the mirror with the help of a spectrometer with included light source.
Secondly you can measure the focused reflectivity. This means, that you have to measure the intensity of light coming out of your light source, hitting the mirror and have to measure the intensity that is focused back by the mirror.

5.1 Pointwise reflectivity with spectrometer

For measuring the pointwise reflectivity we used a ocean optics spectrometer with included light source. The end of the fiber of the spectrometer was placed on a reflectivity standard to calibrate the spectrometer. Afterwards the end of the fiber was placed on the surface of the mirror. In this way you directly get the local reflectivity at this specific point.
With this technique the total reflectivity of the mirror can be determined at several points. It is not possible to distinguish between specular and diffuse reflection. This method is a fast and easy to apply solution to get a first hint about the reflectivity of the mirror but it is not sufficient to test the optical properties of the mirror for the use in the telescope.
To test this property it is needed to measure the focused reflectivity of the mirror, so to determine how much light hitting the mirror is really focused in the focal spot of the mirror. An example of such a measurement is shown in fig. 5.1.

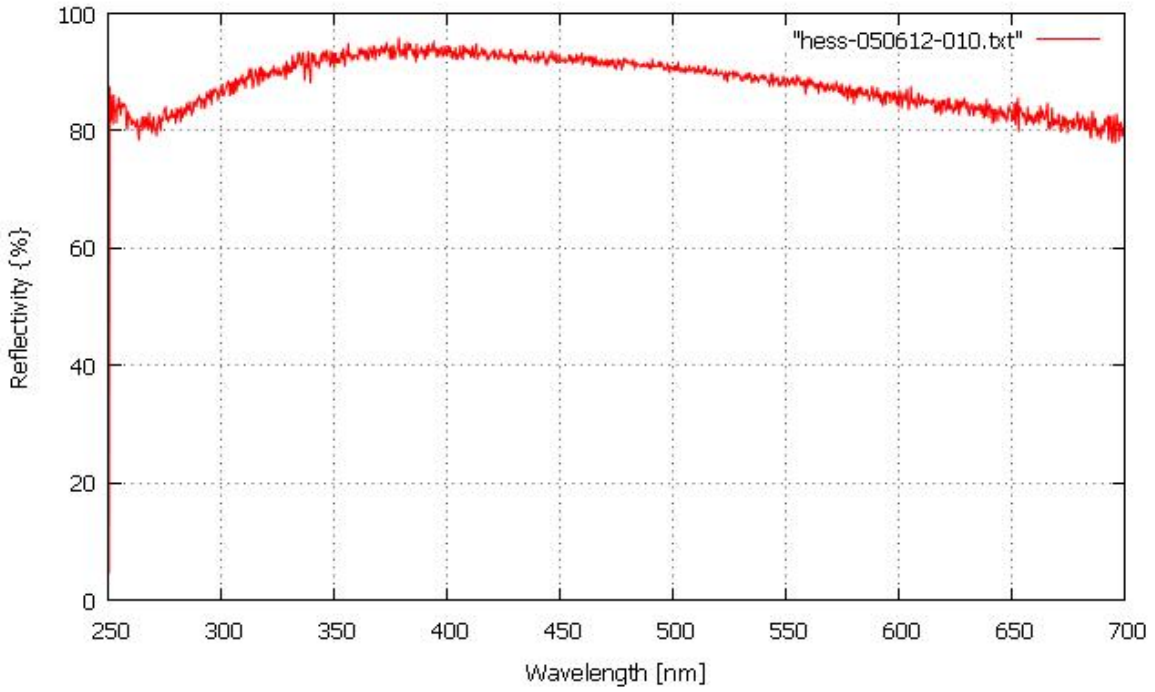

Figure 5.1: Example of a pointwise reflectivity measurement of the HESS A153 mirror.

5.2 Focussed reflectivity

The general idea of the focused reflectivity is based on the equation

$$R_f = \frac{I_R}{I_0} \tag{5.1}$$

with I_R as intensity of the reflected light and I_0 as intensity of the light hitting the mirror. To measure the reflectivity of a mirror two different types of data have to be accomplished. First the intensity that hits the mirror has to be measured and then the one that is reflected back into the focal spot by the mirror. In Erlangen, two different techniques were investigated to perform this measurement.
One possibility is to measure the intensities with a photodiode mounted on a linear stage. A second possibility is to measure these intensities with the help of a CCD camera. Both methods were investigated and will be explained in the following chapter.
Due to the size of the tested mirrors and the large distance that is needed to perform the reflectivity measurements it was not possible to measure the whole intensity that hits the mirror. So this value had to be extrapolated. The intensity of a distant light source on a certain area is decreasing by increasing distance and follows the equation

$$I = \frac{I_0}{r^2} \tag{5.2}$$

with I as the intensity hitting the mirror, I_0 as the base intensity coming from the light source and r as the distance between the light source and the mirror. To extrapolate the

whole intensity that hits the mirror, the intensity hitting a certain area of the mirror has to be summed up to the whole area of the mirror. The best way to solve this problems is to measure the intensity at a certain distance from the light source with a device with known sensitive area and extrapolate the intensity for the whole mirror.
For this technique it is very crucial to know the exact distance between the light source and the mirror. As the same light source was used as for the classical 2f-measurements the position of the real light source is well known (see chapter 3.1.1). To be able to extrapolate the intensity hitting the whole mirror, it is necessary to know the precise light distribution coming out of the light source. The intensity measured at a certain distance from the light source has to be folded with the parametrized light distribution of the used light source.
The light distribution of the light source that was used for all measurements was analyzed. The intensity fluctuation throughout the illuminated area was in the range of 2% or $0.2nA$ photo current on the photodiode used for scanning (see fig. 2.3). So it can be assumed that the used light source is homogeneous. In this case there is no folding of the measured intensities needed to extrapolate the the intensity hitting the mirror.

5.2.1 Focused reflectivity via scanning device

The first approach to measure this intensity was by using a photodiode mounted on a linear table. With such a setup it is possible to scan through the spot coming out of the light source and the PSF coming back from the mirror. So both values can be obtained by the same device which means that there is no need to cross-calibrate different sensors.
The used photodiode had a sensitive area of 7 mm^2. The linear table was equipped with a stepping motor that could be externally controlled by a python script. The stepping motor had a step size of 6.25 μm. This means that a pixel of 2.7 mm would consist of 400 steps. This pixel size was used for all measurements performed with this device.
The scanning device was put in different distances from the light source and the light distribution was measured in a 10 by 10 pixel grid. Out of this the intensity of the light source was extracted and normalized to $\frac{nA}{mm^2 * m_{distance}}$. The measured photocurrent was summed up for all 100 pixels and then divided by 700, which gives the value of the photocurrent per mm^2. To get the distance normalization the equation (5.2) was altered to

$$I_0 = I * r^2 \tag{5.3}$$

As I_0 is the base intensity coming from the light source it is not dependent on the distance of the measurement. So it is expected to be the same for all different distances. Out of this value the intensity on the mirror can be extrapolated very easily. The area of the used mirror and the distance between the mirror and the light source had to be known very precisely. For calibrating the setup the HESS A153 mirror was used. This particular mirror has a diameter of 59.8 cm. So the area of this mirror is $\pi * (299\ mm)^2 = 2,810\ mm^2$.

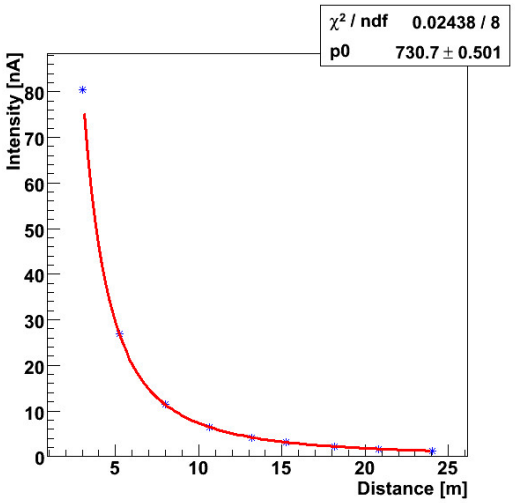

Figure 5.2: Measured intensity of the light source at different distances. The equation (5.2) is fitted with I_0 as free parameter.

The I_0 value for the different measured distances is shown in fig. 5.2. It can be seen that this value is not exactly the same for all measurements, but the variation is about $30\frac{nA}{mm^2}$. This means $\frac{\Delta I_0}{I_0} < 5\%$ which is a acceptable deviation caused by fluctuations within the scanning electronics or the light source itself. For getting a statistically more robust value for I_0 the measured intensity was plotted against the distance. Now the equation (5.2) was fitted on these values with I_0 as free parameter. The plot is shown in fig. 5.3. The fitted value of I_0 is $730.7 \pm 0.5\frac{nA}{mm^2}$.

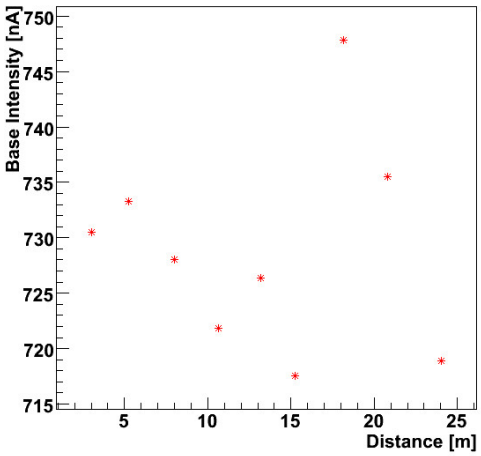

Figure 5.3: Calculated I_0 value for different distances from the light source. The value is normalized to an area of 1 mm^2.

To get the focused reflectivity of the mirror the reflected intensity has to be measured as well. This was done by scanning over the whole PSF of the mirror in the focal spot. A picture of this PSF is shown in fig. 5.4. The intensity for all pixels was summed up and defined as the reflected intensity. As the intensity of the PSF is in the range of some μA and the background is in the range of 0.5 nA the signal to noise ratio is in the order of 10,000 and no background substraction was performed.

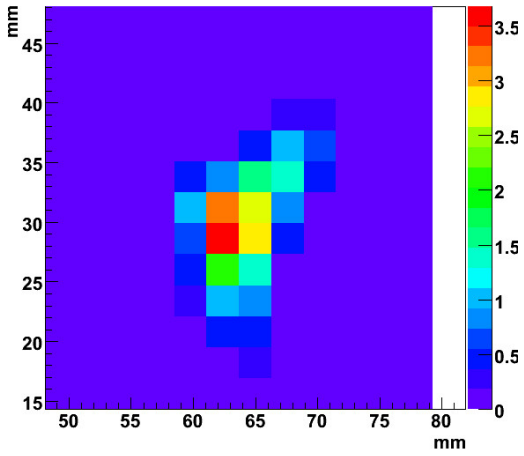

Figure 5.4: Scan of the PSF of the HESS mirror. Intensity is shwon in μA.

The intensity of light that hits the mirror was calculated to 34.4 μA and the intensity of the PSF to 32.9 μA. This leads to a reflectivity of about 95.6%. Out of a pointwise control measurement with the spectrometer a reflectivity of about 85% was expected for the wavelength of the LED (630 nm (see fig. 2.3)). The differences between these two values are not yet completely understood and further research is needed to overcome this discrepancy. One explanation could be an imprecision in the movement of the stepping motor. First measurements show a step-size of 6.05 μm. This would lead to an oversampling of the intensity measurements which has to be corrected. A more precise verification of the step-size has to be performed.
The scanning of the light spot and the PSF is very time consuming. A faster and easier to handle solution would be to measure the intensities with a CCD camera. This possibility was investigated next.

5.2.2 Focused reflectivity via CCD camera

The general idea of measuring the reflectivity with a CCD camera is to take on the one hand a picture of the spot coming out of the light source at different distances and on the other hand one of the PSF. The spot of light is projected on a ground glass and this illuminated ground glass is photographed. The same is done for the PSF of the mirror.
Several problems occurred performing this method. First of all the introduced ground glass is disturbing the signal because of some reflections and scattering inside it. An other problem

is the optics that is in front of the CCD chip. The objective of the camera with its lenses and aperture stop is changing the picture and the measured intensities of the light spot. An example of these effects is shown in fig. 5.5. There can be seen that the homogeneous light distribution coming out of the light source can not be reproduced by the CCD camera. The intensity shows a lambertian profile with some extreme points coming from the behavior of the light inside the ground glass. Effects like scattering, inside reflections and self interference of the light hitting and penetrating the ground glass are not yet understood.

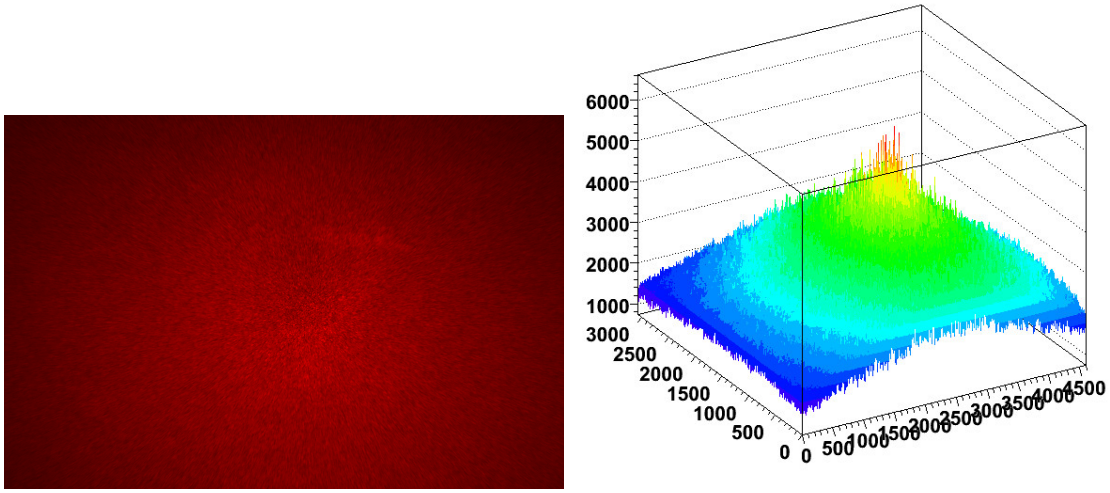

(a) Picture from the camera without any processing

(b) Profile of the light distribution.

Figure 5.5: Picture of the spot coming from the light source taken by the CCD camera in a distance of 6.32 m.

Some other problems can occur due to post processing of the taken pictures and imprecisions of the camera itself. No reflectivity measurements were performed using this commercial CCD camera and further research is needed to compensate all occurring problems.

Chapter 6

Conclusion and outlook

To characterize the optical properties of mirror facets for CTA, the size of the d80 circle is a key-value. The well established system to determine this value is the 2f-method, which was already used to classify mirror facets for IACTs.
We were able to show that an other method called PMD is also able to determine this value. The direct comparison of both methods shows a very good agreement of the results.
Especially during the research and development phase, a further feature of PMD could be used. In contrast to the 2f-measurement PMD can provide spatially resolved data of the surface of the mirror. This can be very helpful to improve the constructing process of the mirror tiles.
PMD uses raytracing to get the PSF out of the spatially resolved surface data from the mirror. This method is not limited to one special point on the opticl axis of the mirror, as it is the case for the 2f-method, but the PSF can be raytraced off-focus and off-axis. This leads to a more realistic simulation of the behavior of the mirrors on the telescope.
To get a realistic simulation of the optical properties of the mirrors, it is as well needed to investigate their behavior with respect to changes in the temperature. Here PMD can again provide a solution, as it is not restricted to the 2f-distance but can be performed in a much more compact setup. So a SWD setup was built up in the climate chamber at DESY Zeuthen and the temperature behavior of different mirror tiles was observed. Since this setup is the very first PMD setup of such a size using four cameras under extreme conditions, unpredicted problems occurred during the measurements. First improvements of the calibration routine were applied and the results are promising. The precision and reliability of the LWD setup is not yet reached.
A drawback of using PMD inside a climate chamber is that the whole setup has to be calibrated for every single temperature step. This calibration routine is very time consuming and not enough data points can be taken in a reasonable time frame. So further systematic studies of the temperature behavior of the setup itself have to be performed to get a better precision of the measurements and to examine the possibility to parametrize the calibration of the setups calibration for different temperatures.

The second very important value to characterize mirror facets is the reflectivity of the mirror. A method to test this is to use a spectrometer and measure the mirror surface pointwise. With this method it is not possible to cover the whole mirror and one can not distinguish

between specular and diffuse reflection. But such a measurement gives very precise results over a wide wavelength range.
We established a method to measure the focused reflectivity of a mirror using a photodiode on a linear table. Measurement results are not yet in full agreement but results are promising. An advantage of this method is, that the focused reflectivity can be observed. This is closer to the real situation on the telescope because the mirrors will focus on the camera of the telescope so only light that is reflected in a focused way can be collected.
One drawback of this method is, that it is very time consuming to scan through the light spot and the PSF. Further methods should be investigated to get a faster measurement. One approach would be to use a CCD camera but a commercially available camera was inapplicable to perform this measurement. Different other solutions would be possible like using a bigger diode or using a combination of a integrating sphere to collect the light and a spectrometer to analyze its intensity.
The now established method is working with a red LED at 630 nm. This LED was chosen because it shows very good homogeneity and emits with sufficiently high intensity. But the mirrors are produced to reflect Cherenkov light with a spectrum between 300 nm and 600 nm. So the currently used method has to be changed to an other wavelength range to be suitable for CTA.

A great benefit for CTA would be an all-in-one test stand to test both critical optical properties in one setup. The possibility of constructing such a setup with a small footprint should be investigated. Including reflectivity measuremens into the SWD-PMD station is tricky. Possible solutions would be to measure inside the setup with a spectrometer and get pointwise reflectivity data out of it or to use the PMD data acquiring process itself to collect intensity data and calculate the reflectivity out of it.

Overall we were able to show that it is possible in Erlangen to measure the most critical optical properties of CTA mirror facets with a high precision also under extreme conditions. Improvements of all existing setups are ongoing to challenge new mirror types or take part in a possible mass test of the mirrors after the prototyping phase is over.

Bibliography

[1] Werner Hofmann et al. official project weppage www.cta-observatory.org

[2] Review of the Mirror Workpackage in Berlin 2011-09-22

[3] MIR WP Calibration Team Mirror Specifications Document

[4] Markus C. Knauer. Absolute Phasenmessende Deflektometrie. PhD thesis, Universität Erlangen-Nürnberg, 2006.

[5] G. Häusler. Verfahren und Vorrichtung zur Ermittlung der Form oder der Abbildungseigenschaften von spiegelnden oder transparenten Objekten. DE 19944354, 1999.

[6] Markus C. Knauer, Jürgen Kaminski, and Gerd Häusler. Phase measuring deflectometry: a new approach to measure specular free-form surfaces. In *Photonics*, Optical Metrology in Production Engineering, SPIE 5457, 2004.

[7] A. Schulz Methods to measure characteristics of mirror facets of Imaging Atmospheric Cherenkov Telescopes Diploma Thesis, University of Erlangen-Nürnberg, 2010.

[8] NIKON GmbH Datasheet of the NIKON D3100

Acknowledgement

I would like to thank all people supporting me in carrying out this thesis. I especially want to thank:

Christian Stegmann for giving me the chance to work on this topic and get in touch with this field of work.
The HESS group Erlangen, for a great work climate. Especially I want to thank Friedrich Stinzing for his supervision, all his support and the proofreading of this thesis. Christopher van Eldik for his enthusiasm, motivating spirit and his helping hands whenever they were needed.
I am grateful for the support of the OSMIN group under Prof. Gerd Häusler. Especially Roman Krobot for his everlasting will to help and all the balcony discussions, Christian Faber for having always an open ear for questions and taking the time to answer them and Evelyn Olesch for her genius ideas how to improve the calibration and for having an answer for all questions.
I would also like to thank the team of DESY Zeuthen, especially Jürgen Bähr, for giving us the chance to work in the climate chamber and for supporting us every minute we have been in Zeuthen.
Beside my colleagues my thanks also go to my family.
My mother for make my good school education possible and for her everlasting faith.
My wife for her support, her love, the final proofreading of this thesis and her from time to time needed kick in the backside.
I would like to thank my parents in law for giving me a home and making it possible to concentrate on my studies.
Last but no least my gratitude goes to my little daughter. The sleepless nights she provided were a good training for writing this thesis. Her unbelievable smile is always a new motivation to go on.

Persönliche Erklärung

Hiermit erkläre ich, dass ich die Arbeit selbstständig angefertigt und keine anderen als die angegebenen Hilfsmittel verwendet habe.

Erlangen, 09.07.2012

André Wörnlein